2003-09

Design and optimization of a 600-KJ railgun power

Warnock, Dwight S.

Monterey, California. Naval Postgraduate School

NAVAL
POSTGRADUATE
SCHOOL

MONTEREY, CALIFORNIA

THESIS

DESIGN AND OPTIMIZATION OF A 600-KJ RAILGUN POWER SUPPLY

by

Dwight S. Warnock

September 2003

Thesis Advisor:	Robert W. Ashton
Second Reader:	William B. Maier II

Approved for public release; Distribution is unlimited

THIS PAGE INTENTIONALLY LEFT BLANK

REPORT DOCUMENTATION PAGE			Form Approved OMB No. 0704-0188
Public reporting burden for this collection of information is estimated to average 1 hour per response, including the time for reviewing instruction, searching existing data sources, gathering and maintaining the data needed, and completing and reviewing the collection of information. Send comments regarding this burden estimate or any other aspect of this collection of information, including suggestions for reducing this burden, to Washington headquarters Services, Directorate for Information Operations and Reports, 1215 Jefferson Davis Highway, Suite 1204, Arlington, VA 22202-4302, and to the Office of Management and Budget, Paperwork Reduction Project (0704-0188) Washington DC 20503.			
1. AGENCY USE ONLY *(Leave blank)*	**2. REPORT DATE** September 2003	**3. REPORT TYPE AND DATES COVERED** Master's Thesis	
4. TITLE AND SUBTITLE: Design and Optimization of a 600-KJ Railgun Power Supply			**5. FUNDING NUMBERS**
6. AUTHOR(S) Warnock, Dwight S.			
7. PERFORMING ORGANIZATION NAME(S) AND ADDRESS(ES) Naval Postgraduate School Monterey, CA 93943-5000			**8. PERFORMING ORGANIZATION REPORT NUMBER**
9. SPONSORING /MONITORING AGENCY NAME(S) AND ADDRESS(ES) N/A			**10. SPONSORING/MONITORING AGENCY REPORT NUMBER**
11. SUPPLEMENTARY NOTES The views expressed in this thesis are those of the author and do not reflect the official policy or position of the Department of Defense or the U.S. Government.			
12a. DISTRIBUTION / AVAILABILITY STATEMENT Approved for public release; Distribution is unlimited			**12b. DISTRIBUTION CODE** A

13. ABSTRACT (maximum 200 words)

The purpose of this thesis is to explore the design options for a 1.2-m railgun power supply capable of accelerating a 150-g to 250-g projectile to 1000 m/s. In order to accomplish this task a MATLAB model will be constructed to conduct trade-off studies between various power supply configurations in an attempt to maximize the system performance. The final design shows that by distributing the system capacitance between four equal size banks and firing them sequentially the total system capacitance can be reduced by more than half. Because the capacitor banks are fired sequentially, the current pulse is length-ened resulting in more efficient use of the barrel. The final benefit of using a multiple-bank system is that the individual bank currents are reduced by a factor of four over the single-bank scenario. By reducing the bank currents solid-state switches are now an affordable option further improving the system performance. By applying a systematic approach to optimizing the power supply this study has shown that the energy required to accelerate a 172-g projectile to 1000 m/s can be reduced from 1.3 MJ in the single-bank scenario to 600 KJ by distributing the capacitance over four equal sized banks.

14. SUBJECT TERMS railgun, solid-state switches, pulsed power supply, electromagnetic launch, thyristors, spark-gap switches, naval railgun			**15. NUMBER OF PAGES** 103
			16. PRICE CODE
17. SECURITY CLASSIFICATION OF REPORT Unclassified	**18. SECURITY CLASSIFICATION OF THIS PAGE** Unclassified	**19. SECURITY CLASSIFICATION OF ABSTRACT** Unclassified	**20. LIMITATION OF ABSTRACT** UL

NSN 7540-01-280-5500

Standard Form 298 (Rev. 2-89)
Prescribed by ANSI Std. 239-18

THIS PAGE INTENTIONALLY LEFT BLANK

Approved for public release; Distribution is unlimited

DESIGN AND OPTIMIZATION OF A 600 KJ RAILGUN POWER

Dwight S. Warnock
Lieutenant, United States Navy
B.S., United States Naval Academy, 1995

Submitted in partial fulfillment of the
requirements for the degree of

MASTER OF SCIENCE IN ELECTRICAL ENGINEERING

from the

NAVAL POSTGRADUATE SCHOOL
September 2003

Author: Dwight S. Warnock

Approved by: Robert W. Ashton
Thesis Advisor

William B. Maier II
Second Reader/Co-Advisor

John P. Powers
Chairman, Department of Electrical Engineering

THIS PAGE INTENTIONALLY LEFT BLANK

ABSTRACT

The purpose of this thesis is to explore the design options for a 1.2-m railgun power supply capable of accelerating a 150-g to 250-g projectile to 1000 m/s. In order to accomplish this task a MATLAB model will be constructed to conduct trade-off studies between various power supply configurations in an attempt to maximize the system performance. The final design shows that by distributing the system capacitance between four equal size banks and firing them sequentially the total system capacitance can be reduced by more than half. Because the capacitor banks are fired sequentially, the current pulse is lengthened resulting in more efficient use of the barrel. The final benefit of using a multiple-bank system is that the individual bank currents are reduced by a factor of four over the single-bank scenario. By reducing the bank currents solid-state switches are now an affordable option further improving the system performance. By applying a systematic approach to optimizing the power supply this study has shown that the energy required to accelerate a 172-g projectile to 1000 m/s can be reduced from 1.3 MJ in the single-bank scenario to 600 KJ by distributing the capacitance over four equal sized banks.

THIS PAGE INTENTIONALLY LEFT BLANK

TABLE OF CONTENTS

LIST OF FIGURES

LIST OF TABLES

THIS PAGE INTENTIONALLY LEFT BLANK

ACKNOWLEDGMENTS

I would like to thank my loving and supportive wife Dana, who has made countless sacrifices allowing me to devote my full attention to this work. I would also like to acknowledge Robert W. Ashton for his insight and technical assistance in completing this thesis. I have also been honored with the opportunity to work with William B. Maier II. His guidance, encouragement, and inexhaustible willingness to teach have helped me to gain a better perspective on the finer points of railgun operation and design. Additionally, I would like to thank Mark Crawford at the Institute for Advance Technology for the information and tour of the railgun facility at the University of Texas at Austin. Finally, I would like to thank Todd Hansen at Silicon Power Corporation for the simulation results and data he provided for their products. His keenness and eagerness to help has enlightened my own knowledge solid-state devices.

THIS PAGE INTENTIONALLY LEFT BLANK

EXECUTIVE SUMMARY

This thesis explores the power supply options for a 1.2-m railgun currently residing at the Naval Postgraduate School (NPS) in Monterey, California. The near-term focus of the railgun research at NPS is on maintaining electrical contact between the rails and the projectile's armature. The long-term goal is to make sufficient improvements to the barrel erosion characteristics so that the railgun can become a viable weapon for the Navy's future all-electric ships. In order to continue the research here at NPS, it is necessary to conduct the experiments on electrical contact and rail erosion under conditions that are representative of a full-scale system. The Center for Naval Analysis (CNA) has estimated that the full-scale railgun should have the following characteristics: a 10-m barrel, a muzzle velocity of 2.5 km/s, and a projectile weighing 20 kg. It has been determined that accelerating a projectile weighing 172-g to a velocity of 1000 m/s using a 1.2-m barrel closely approximates the full-scale railgun with regard to current density through the armature.

Only two practical alternatives exist to the meet the power requirements for the system. The first and least mature alternative is the compensated pulse alternator or "compulsator". A compulsator is similar in construction to a three-phase alternator, but has a set of internal windings used to reduce the machine's inductance. By reducing the output inductance, the machine is able to supply a rapidly rising sinusoidal current pulses. These current pulses are then rectified using Silicon Controlled Rectifiers (SCR) to provide a DC output. Compulsator's show great promise for the full-scale railgun, but are too expensive and immature as a technology to be used here at NPS.

The other option for this design is a capacitor-based system. Capacitor technology is the most commonly used and most mature technology found in railgun power supplies. By connecting a large number of capacitors in parallel and controlling their discharge through an inductor and a set of switches, it is possible to produce a large peak current that it suitable for powering a railgun. Because capacitors are more reliable and readily available, this will be a capacitor-based design.

A MATLAB model was developed to facilitate conducting trade-off studies between four possible configurations. The goal was to determine the best arrangement for the capacitor banks while at the same time minimizing the total system capacitance. It was shown that by sequentially firing four equal banks of capacitors the total system capacitance could be reduced. The single-bank case required a capacitance of 21.58 mF while the multiple-bank case required 9.96 mF. An additional advantage of the multiple-bank case over the single-bank case is the peak current is reduced from 626 kA to 567 kA. The final advantage of the multiple-bank case is that the current density in the armature is reduced from 39.1 kA/cm^2 to 35.5 kA/cm^2. The reduction in current density should result in improved barrel erosion characteristics.

Further trade-off studies were conducted to optimize the components selected for building the multiple-bank configuration. The characteristics of the parts selected in this set of trade-off studies were used to build a PSpice model that more accurately simulated the power supplies performance. The results from the PSpice model were consistent with the MATLAB model. It is recommended that one bank from the multiple-bank model is built and tested to confirm the results and assumptions of this thesis.

I. INTRODUCTION

A. PURPOSE

This thesis supports ongoing research conducted at the Naval Postgraduate School to support the full-scale development of an ElectroMagnetic Launch (EML) gun, commonly known as a railgun. This type of gun would be capable of taking full advantage of the Navy's efforts to develop and field an all-electric ship. The purpose of this thesis was to research the power supply options for an existing 1.2-m railgun that resides in the Naval Postgraduate School's physics department. In the course of developing a recommended design for this power supply, it was be necessary to conduct trade-off studies on its various components to maximize performance while minimizing the total system cost.

B. THE PUSH FOR NAVAL RAILGUNS

1. CNO Visibility

The Chief of Naval Operation (CNO) outlined his vision for the future capabilities of the Navy in *Sea Power 21,* an overarching document to be used as a guide to developing future naval technologies and capabilities. In this document the CNO identified three core capabilities of the Navy: sea strike, sea shield, and sea basing [1]. A railgun has the capability to play an important part in all of these areas by providing time-sensitive strike using large caliber guns and to provide force protection and area denial using medium caliber guns. Large caliber guns could also be a key enabler to sea basing and the Marine Corps' Operational Maneuver From The Sea (OMFTS) concept by allowing shore units the luxury of large caliber weapons without the weight that results in slow moving forces.

On November 15, 2002 the CNO gave the following direction to PMS 405 [2]:

> I AM DIRECTING NAVSEA TO REDESIGNATE PMS 405 THE NAVY ELECTRIC WEAPONS OFFICE AND INCORPORATE WITHIN IT AN ELECTROMAGNETIC WEAPONS DIVISION RESPONSIBLE FOR MANAGING THE FULL SCALE PROOF OF CONCEPT RAIL GUN ….
>
> …PMS 405 WILL ALSO BE RESPONSIBLE FOR COORDINATING WITH OTHER PROGRAM OFFICES (ESPECIALLY PEO SHIPS AND PEO IWS) TO ENSURE THAT DDX AND FOLLOW ON IPS SHIPS ARE DESIGNED TO THE MAXIMUM EXTENT FEASIBLE TO

ACCOMMODATE FORWARD AND BACKFIT OF HIGH POWER ELECTRIC WEAPONS…

…I AM DIRECTING NAVSEA TO WORK WITH ONR AND DARPA TO DEVELOP A COORDINATED PLAN TO DEMONSTRATE A FULL SCALE EM GUN AND HYPERSONIC GUIDED PROJECTILE.

From the above statement it is clear that the leadership of the Navy is serious about developing electric weapons, including railguns for future employment on Navy warships.

2. Marine Corps Surface Fire Support

The Marine Corps has set a range of 200+ NM as a requirement for Naval Surface Fire Support (NSFS). Table 1 shows the parameters of a notional railgun purposed by the Center for Naval Analysis (CNA) and Table 2 is a comparison between the CNA railgun projectile, the 5″ Extended Range Guided Munitions (ERGM) round and the 155-mm Long Range Land Attack Projectile (LRLAP) [3]. The ERGM and LRLAP rounds and their associated gun systems are both being considered for use on DD(X).

Flight Mass	15 kg
Launch Velocity	2.5 km/s
Muzzle Energy	63 MJ
Breech Energy	150 MJ
Peak Acceleration	45 kgee
Range	200 NM – 300 NM
Energy on Target	16.9 MJ

Table 1. CNA Notional Railgun. (After Ref.3.)

Table 2 shows a vast improvement in performance of the CNA notional railgun when compared to the ERGM and LRLAP rounds. It is significant to note that the CNA gun is the only system capable of meeting the Marine Corps future NSFS requirements. Also of some significance is the weight saving when compared to the other rounds. The

total weight for the ERGM round is 150 lbs (110 lbs for the projectile and 40 lbs for the powder charge) and similarly the total weight for the LRLAP is 350 lbs. Because the railgun round is a kinetic energy round traveling at high speed it does not contain explosives, has a much smaller weight, and delivers over twice the energy to the target as the LRLAP round. It derives additional weight savings from the fact that it is an EML round and requires less than three gallons of fuel to power the electric generators per launch.

	5″ ERGM	155-mm LRLAP	CNA Notional Railgun
Range (NM)	43	63	250
Time of flight (min)	6	6	6
Weight (lbs)	110 + 40	260 + 90	44 + 3 gal. Fuel
Energy on target (MJ)	2.2	7.8	16.9

Table 2. Comparison of CNA Railgun, ERGM, and LRLAP performance. (After Ref. 3.)

3. Integrated Power System

The Navy's decision to install an Integrated Power System (IPS) with electric drive on the DD(X) has opened the possibility for the use of electric weapons onboard these ships. Conventional propulsion systems locked over 80 percent of the ship's total power in the propulsion train. In an IPS the power that would normally be reserved for propulsion only can now be made available for electric weapons as shown in Fig. 1.

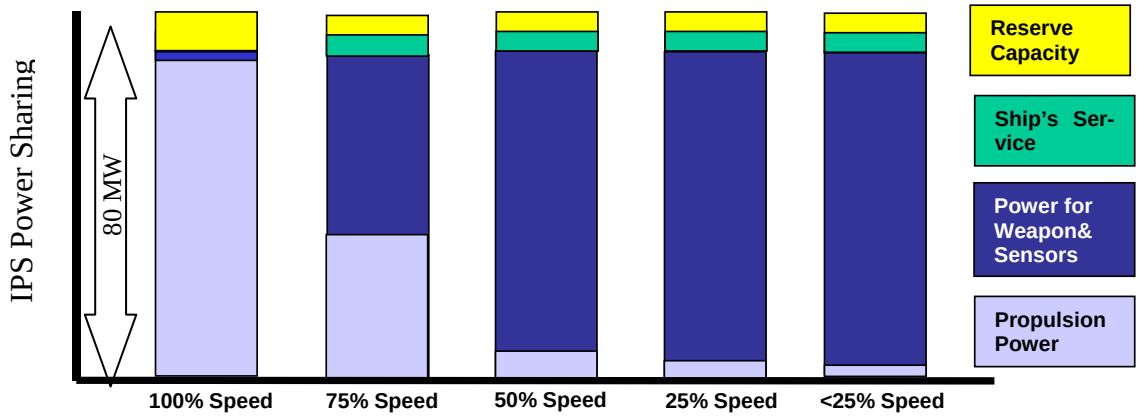

Figure 1. IPS Power Sharing. (From Ref. 3.)

The estimated power required for the CNA railgun is 20 to 40 MW to achieve a firing rate of 6 to 12 round per minute. It is important to note that at greater than 75% of

full speed a significant percentage of the ship's power must now be dedicated to propulsion which results in limited firing rates for electric weapons.

C. CHALLENGES FOR NAVAL RAILGUNS

1. Rail Erosion

Current operating railguns used for research exhibit severe rail damage in the form of gouging and erosion under the high current and heat conditions at the rail-projectile interface. Figure 2 is an example of damage due to gouging. The result is that the rail/barrel life is reduced to the point that it is not a viable weapons system. The Institute of Advanced Technology at the University of Texas has solved the problem of gouging, but rail erosion remains a significant issue. In order to further understand the interactions at the rail-projectile interface, it is necessary to study the problem under conditions of current, velocity and temperature similar to the full-scale system. Solving this problem is the focal point of the research being conducted here at the Naval Postgraduate School, and the reason for designing and building this power supply for an NPS 1.2-m gun.

Figure 2. Rail gouging. (From Ref. 4.)

2. Projectile Guidance

The standard for modern weapon systems has become pinpoint accuracy with near 100 percent reliability. To achieve that with a kinetic energy round fired at 2.5 km/s out to a range of 250 NM will present some significant guidance and control issues. Entering offsets to compensate for wind variation over a 250 NM range is not a reasonable

solution. In order to achieve the kind of accuracy and precision needed to be an effective weapon requires in-flight correction to ensure projectile to target contact. The simplest solution would be GPS guidance. The peak launch acceleration of the projectile is 45 kgee. To date GPS systems have demonstrated the ability to survive launch acceleration of only one-third the predicted CNA railgun launch acceleration. Other solutions have been suggested, such as a satellite guidance system for "exo" then "endo"-atmospheric projectiles, but it is clear there is not a simple solution to this problem.

3. Pulsed Power Supply

A considerable amount of research is being done on the types of power supplies that might best be suited for use in a naval railgun. Historically, all weapons systems were self-contained and included their own power conditioning components. The operation of these systems did not affect the ship's propulsion because they are operated in isolation from the rest of the ship's functions. IPS, as discussed earlier, has made it feasible to place high-power electric weapons on ships. The power requirements associated with all electric weapons are forcing designers to make choices between ship's speed and the increased performance offered by these systems. As one might imagine when dealing with a system that requires 20 to 40 MW of power, the size and weight of those systems as well as their location will have a major impact on the overall ship design. It is for this reason that engineers are conducting in-depth research in order to try to minimize the size and weight of railgun power supplies.

D. THE NPS RAILGUN

1. Electromagnetic (EM) Gun Theory

The basic theory behind railguns was established around 1901 when Birkeland developed the "Patent Electric Cannon." [5] The basis for this technology is founded on the Lorentz Force, which describes the interaction between electric current and magnetic fields, and is given by

$$\vec{F} = q(\vec{v}_d \times \vec{B}) . \tag{1.1}$$

Electric current flows down the rail creating a magnet field between the rails. The projectile completes the circuit path resulting in current flow with a drift velocity ($\vec{v}_d$)

and a perpendicular component to the magnet field ($\vec{B}$) resulting in a force ($\vec{F}$) on the projectile. Figure 3 illustrates this interaction.

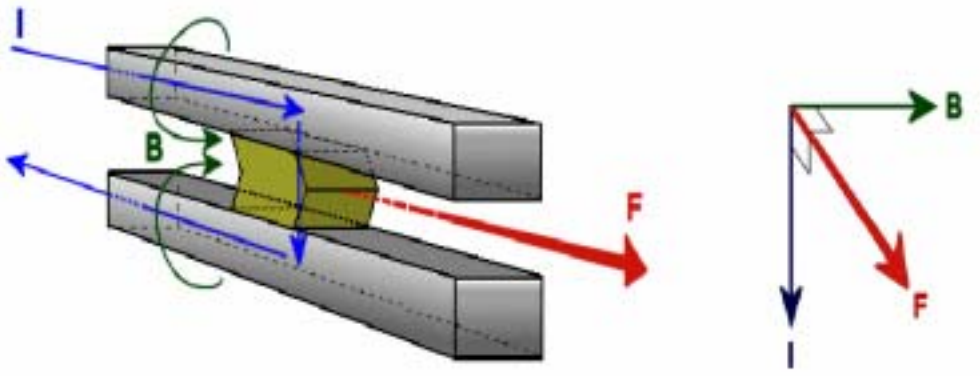

Figure 3. (Left) Current and magnetic field interaction; (Right) Lorentz Law. (From Ref. 6.)

The following discussion is also found in a master's thesis written by Allen Faliciano that characterizes the power supply requirements for the physics department's 1.2-m railgun [6]. The interaction between the projectile and the rails can be approximately characterized by examining the magnitude of the Lorentz Force

$$F = qv_d B, \tag{1.2}$$

where q is charge, v_d is the magnitude of the drift velocity associated with the current, and B is the magnitude of the magnetic field between the rails. The amount of charge transfer through the projectile and across the magnetic field can be expressed as

$$q = It = I\frac{l}{v_d}, \tag{1.3}$$

where l is the distance traveled across the projectile, as shown in Fig. 4.

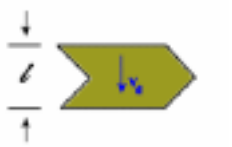

Figure 4. Drift velocity and length through the projectile. (From Ref. 6.)

Substituting Equation 1.3 into Equation 1.2 and differentiating along the length l yields

the following equation

$$dF = v_d B\, dq = \left(I \frac{dx}{v_d} \right)(v_d)B = BI\, dx\,. \tag{1.4}$$

By applying the Biot-Savart Law for a semi-infinite straight wire, it can be shown that the magnetic field produced by the current in the wire is

$$B = \frac{\mu_o I}{4\pi r}, \tag{1.5}$$

where μ_o is the permeability of free space and r is the radial distance from the center of the wire. From this point it is necessary to make two assumptions: 1) the current flows only through the center of the rails, and 2) the magnetic characteristics of rectangular rails are approximated by long circular wires, as illustrated in Fig. 5.

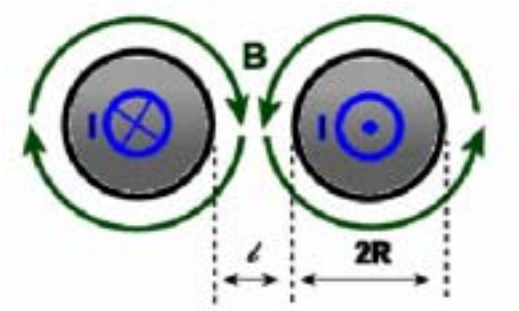

Figure 5. Magnetic fields created by current in the rails. (From Ref. 6.)

By substituting Equation 1.5 into Equation 1.4 and integrating, the Lorentz force between the rails is approximately

$$F = \frac{\mu_0 I^2}{4\pi} \int_R^{R+l} \left(\frac{1}{x} + \frac{1}{2R + l - x} \right) dx\,. \tag{1.6}$$

Evaluating the integral and simplifying yields

$$F = \frac{\mu_0 I^2}{4\pi} \ln\left[\frac{(R+l)^2}{R^2} \right]. \tag{1.7}$$

From Equation 1.7 the term L' is derived

$$L' \equiv \frac{\mu_0}{2\pi} \ln\left[\frac{(R+l)^2}{R^2}\right]. \tag{1.8}$$

It is important to note that L', which has units of H/m, is not an actual inductance of the system, but rather a magnetic field factor. This field factor is solely dependant on the geometry of the railgun itself and does not change once the gun has been constructed. By substituting Equation 1.8 into Equation 1.7 the Lorentz Force on the projectile can be expressed with the following simple equation:

$$F = \frac{1}{2} L' I^2. \tag{1.9}$$

Dividing through by the mass of the projectile in Equation 1.9 will result in an equation for acceleration of the projectile:

$$a = \frac{1}{2m} L' I^2. \tag{1.10}$$

Equation 1.10 can then be integrated with respect to time to produce the velocity equation. Then the velocity equation can be integrated with respect to time to produce the position or barrel displacement equation. In order to obtain an exact solution to these equations, it is necessary to know the initial velocity and position of the projectile.

2. Characteristics of the NPS Railgun

The physics department at the NPS has a 1.2 m railgun designed as a student thesis by Michael M. Lockwood and shown in Fig. 6 [7].

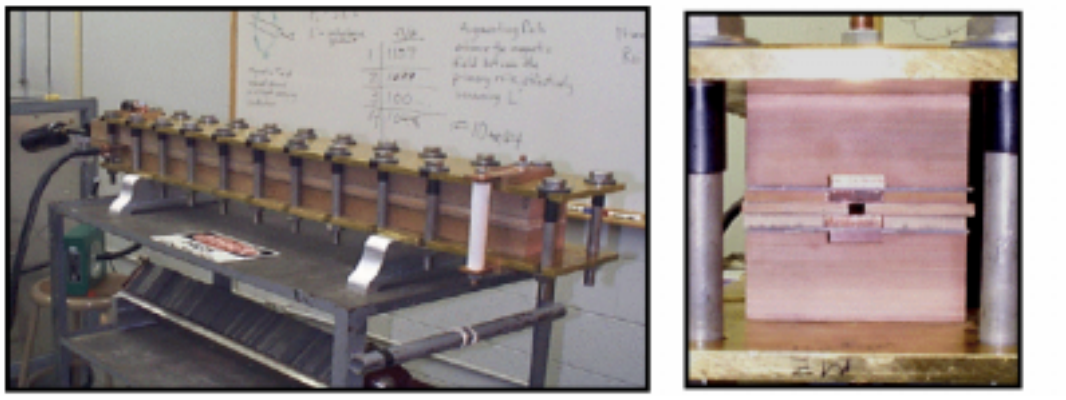

Figure 6. (Left) NPS 1.2 m railgun; (Right) Muzzle view. (From Ref. 7.)

One characteristic of the NPS railgun not previously discussed is the use of augmenting rails. These rails are located parallel to the inner contact rails and enhance the magnetic field between the inner rails. This results in an increase in L' and a corresponding increase in projectile speed for a given current. Figure 7 illustrates the use of augmentation rails.

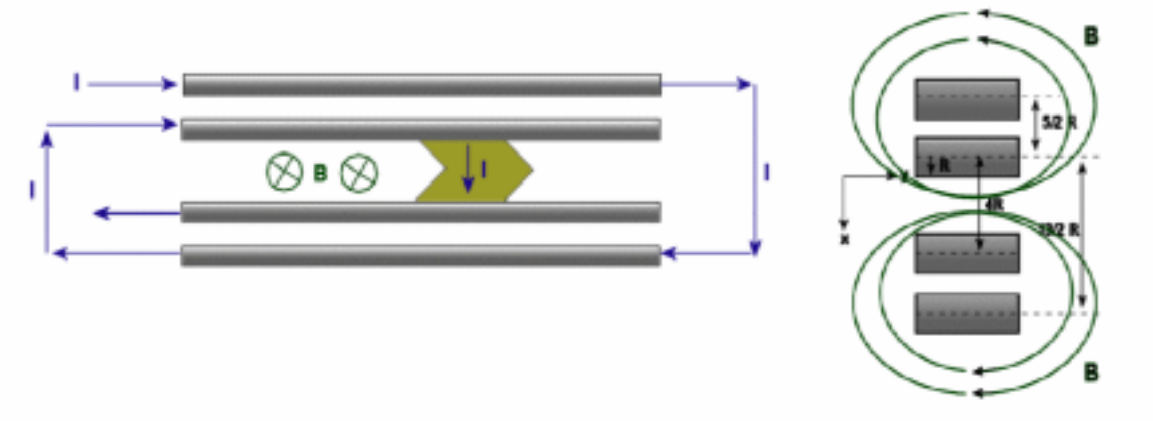

Figure 7. (Left) Augmentation rail arrangement; (Right) Muzzle view showing the relative spacing between inner and out rails. (After Ref. 7.)

When examining the right side of Fig. 7, it is important to note that all the distances are defined in terms of the rail radius (*R*), but the rails themselves are actually rectangular in shape. There are two important issues: 1) the validity of the round rail assumption, and 2) changing the inner rail separation or bore width without changing the relative spacing of the rest of the rails since they are all referenced to *R*. The round rail issue can be addressed by first integrating over the surface area of the projectile to determine the magnitude of the magnetic field component that is perpendicular to the current through the projectile. Once the magnetic field value for the round rail case is determined, it can be compared to the ideal case where the entire magnetic field is perpendicular to the current flow through the projectile. This procedure indicates that the round rail assumption caused only about a one percent difference in the estimated magnetic field strength in the region between the primary rails.

In most cases it would be desirable to change the bore width without changing the separation between the inner and outer rails of the gun. The preferred spacing for the outer rails is as close to the inner rails as is permitted by the insulator separating them. In

order to change the bore width without changing the other rail spacing in the calculation of L', the rail geometry must be defined in a different manner than it is done in Fig. 7. First look at the equation resulting from the relationships in Fig. 7,

$$F = \frac{\mu_o I^2}{4\pi} \int_R^{3R} \left(\frac{1}{x} + \frac{1}{4r - x} + \frac{1}{\frac{5}{2}R - x} + \frac{1}{\frac{13}{2}R - x} \right) dx . \tag{1.11}$$

The first and third terms inside the integrand represent the contribution from the upper set of rails. Keeping those terms and applying superposition to account for the bottom rails results in the following equation:

$$F = \frac{\mu_o I^2}{2\pi} \int_R^{3R} \left(\frac{1}{x} + \frac{1}{\frac{5}{2}R - x} \right) dx . \tag{1.12}$$

From further examination it can be seen that the spacing between the centerline of the top two rails is equal to $5R/2$. This distance is equal to the radius of both rails plus some separation, in this case $R/2$, for a total of $5R/2$. By defining $R = w/2$, where *w* is the rail width, *s* is the spacing between the inner and outer rails and *b* is the bore width Equation 1.12 can now be expressed as

$$F = \frac{\mu_o I^2}{2\pi} \int_{\frac{w}{2}}^{\frac{w}{2}+b} \left(\frac{1}{x} + \frac{1}{(w+s) - x} \right) dx . \tag{1.13}$$

Defining L' in the same manner as Equation 1.8 and leaving it in the integral form to be evaluated numerically in a MATLAB results in the following equation

$$L' \equiv \frac{\mu_o}{\pi} \int_{\frac{w}{2}}^{\frac{w}{2}+b} \left(\frac{1}{x} + \frac{1}{(w+s) - x} \right) dx . \tag{1.14}$$

What is of importance is that now the values of rail width, separation, and bore width can be varied independently to more accurately model any gun, including the existing NPS gun.

3. Assumptions and Performance Goals

So far the only parameter of the rail gun that has been discussed is the rail geometry and its effect on L'. Once L' and the input current are obtained, the gun can be modeled accurately. The current pulse and friction are the only other aspects of the gun left to cover. The first assumption with regard to current is that it flows through the center of the rails, as previously discussed, and that it is distributed uniformly over the contact area between the rails and the projectile. The actual current distribution in the rails is more accurately represented in Fig. 8. Including this effect in the model would cause an increase in resistance and complicate the calculation of the magnetic field between the rails and L'.

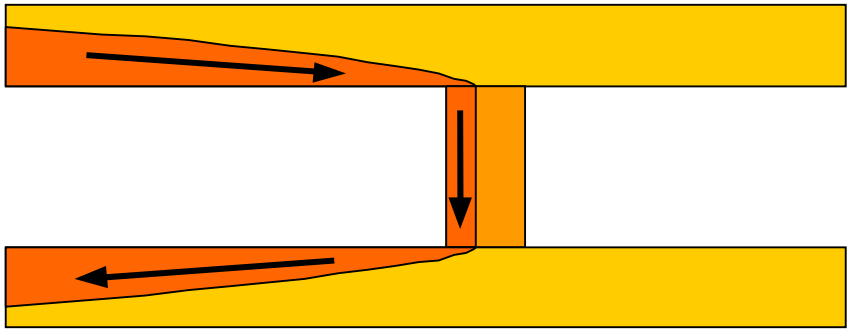

Figure 8. Current distribution in the rails and projectile. (From Ref. 8.)

It is also known that the resistance of the rails and their inductance varies as the projectile travels down the barrel. Similar to the effect seen in linear motors, the change in inductance as the projectile moves down the barrel will induce a voltage on the rails known as back ElectroMagnetic Force (EMF). This voltage is equal to $I\,dL/dt$, where dL/dt is the change in barrel inductance over time caused by the projectile movement, and I is the current [8]. Figure 9 shows these effects plotted for a 1.2-m gun similar to the one in Fig. 6, but with a wider bore and a muzzle velocity of 1000 m/s. Because the NPS railgun barrel is only 1.2 m long, it is assumed that these affects will be small and are therefore neglected.

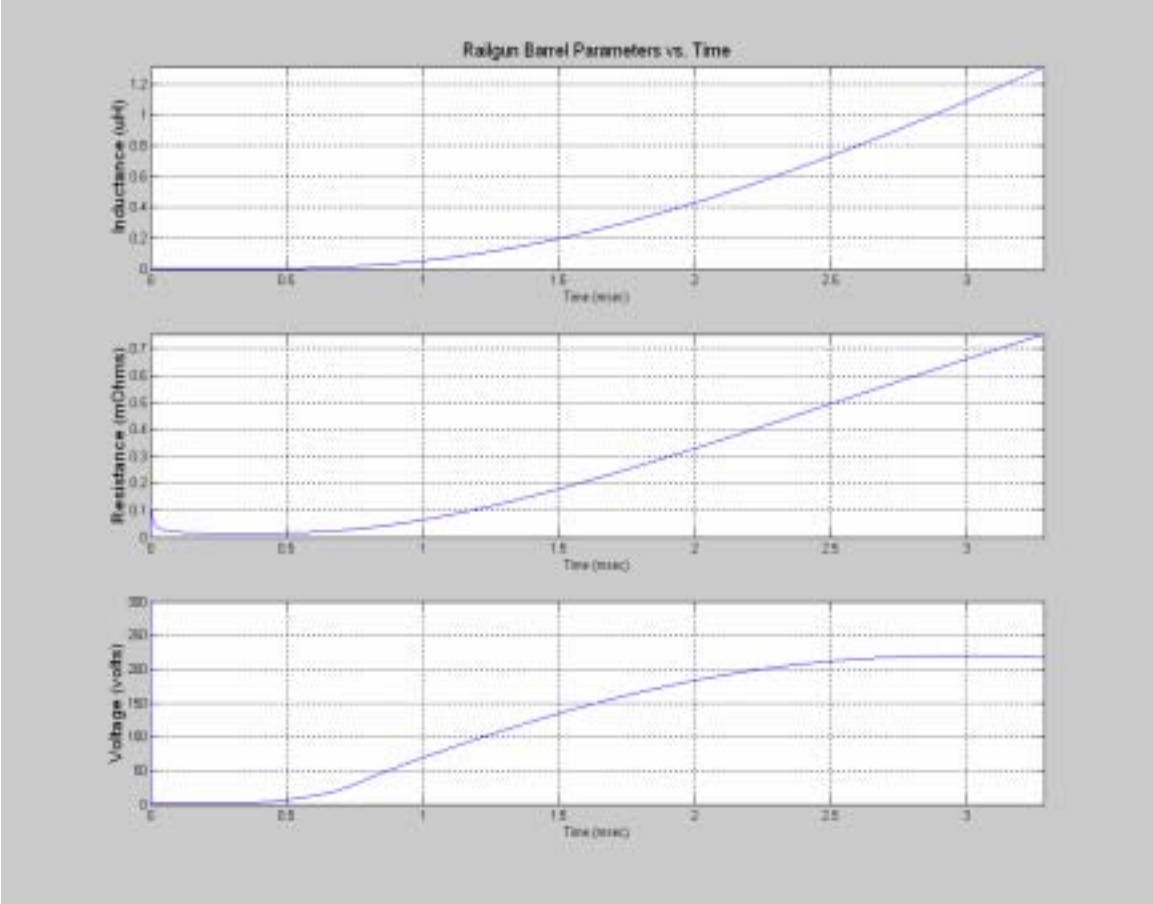

Figure 9. 10-m railgun inductance, resistance and inductance profiles vs. time.

Current research at NPS is pursuing a method to maintain contact between the rails and the projectile by coating the rails with a conducting lubricant and then injecting the projectile into the breech. Because the projectile is entering the breech with an initial velocity, the effects of static friction are neglected. Dynamic friction is calculated from the following formula:

$$F_{friction} = \frac{\nu A u}{\Delta t}, \tag{1.15}$$

where ν is the SI unit symbol for viscosity of the fluid in Poiseuille, A is the contact surface between the rail and the projectile in units of m^2, u is the projectile speed in units of m/s, and Δt is the fluid thickness measured in units of m. Current experimentation on a 4″ railgun calls for the rail spacing to be in the range of 0.5 to 1 mils or 12.7 to 25.4 microns wider than the projectile to ensure good contact as the projectile travels down the

barrel. Taking the worst-case scenario of 12.7 microns and dividing that over the two projectile contact surfaces results in a fluid thickness of 6.35 microns. The paste that is currently used to coat the rails is 65% silver and 35% mineral oil, and has a viscosity similar to that of heavy grade motor oil, which is 1000 cP at 20°C. At the present time there is no good model for rail heating in this gun, but it can be said with great certainty that the rails will be hotter than 20°C causing the viscosity of the paste to decrease. In the absence of a numerical model or experimental measurement, it is assumed that the paste will have a viscosity similar to that of lightweight motor oil once it is heated, which is 65 cP at 20°C.

The desire of the physics department is to accelerate a projectile with a mass between 150 g and 250 g to a speed of 1000 m/s, while maintaining the current density in the projectile and the muzzle energy as low as possible. There are several key interdependencies to keep in mind when trying to optimize the power supply and the gun, and are listed below:

a. *Increasing* the current will *increase* the current density and the projectile acceleration.

b. *Increasing* the projectile surface area will *increase* the projectile mass while *decreasing* the projectile acceleration and maximum current density.

It is also desirable to use the entire barrel length to accelerate the projectile rather than trying to transfer the energy from the power supply to the projectile in a short period of time. Using the entire barrel will help to keep the current densities lower in the projectile. This will improve the barrel life by utilizing more of the barrel for energy transfer from the power supply to the projectile. Table 3 is a summary of tentative desired parameters and assumptions for the NPS railgun.

Before continuing, it is necessary to further clarify the inputs from Table 3. The desired muzzle velocity requires little explanation, as it is the minimum acceptable projectile velocity on exit of the barrel. Barrel length, bore width, rail spacing and silver paste viscosity are all either assumed or are characteristics inherent to the gun and, will therefore be treated as constants for this design.

Barrel length: 1.2 m	Muzzle Velocity: 1000 m/s	Bore width: 1.6 cm
Inductance*: 2.5 μH	Resistance*: 0.003 Ω	L' based on Eq. 1.13: 1.1 μH/m
Voltage: 10 kV –18 kV	Projectile Density: 13.4 g/cm^3	Projectile weight: 150-250 g
Rail spacing: 0.5-1.0 mils wider than the projectile	Silver paste viscosity: 65 cP	Maximum projectile current density: 40 kA/cm^2

* Estimated values for the resistance and inductance of the gun and associated cabling based on data collected in Ref. 7

Table 3. Desired parameters for the NPS railgun (After Ref. 7.)

The inductance and resistance values from Table 3 are assumed to be the minimum attainable for this rail configuration and thereby set the minimum values for use in the model. The projectile density is based on a Cu-W alloy. This implies that for a given size the projectile weight can only be changed by removing mass or by changing the projectile composition.

Now that the basics railgun theory has been established, the following chapters will use this information to develop a model and produce a design for a 1.2-meter railgun power supply. Chapter II covers the possible alternative power supply and develops a MATLAB model used to conduct trade-off studies. In Chapter III the results from Chapter II are used to determine suitable system components for the construction of the power supply. Chapter IV contains a PSpice simulation based on the components listed in Chapter III, a price list and a cost breakdown. The final section of Chapter IV provides a summary of the results and a recommendation for continued research. Also included are Appendix A, the MATLAB code developed in Chapter II, and Appendix B, a more detailed discussion of the single-bank model.

II. PULSE FORMING NETWORKS

This chapter will look at two of the primary technologies available to power rail-guns and compare their suitability for the NPS project. Once a technology is selected, a model will be constructed for the purpose of conducting trade-off studies. This model will be used to estimate the power supply size and predict the gun and power supply combined performance. The result of this chapter will be a recommended configuration for the final design.

A. CAPACITORS VS. COMPENSATED PULSED ALTERNATORS

The reason for Pulse Forming Networks (PFN) is to approximate the ideal current pulse for an EML projectile. In order to reduce the peak acceleration and get the maximum use out of the barrel, the ideal current pulse would be one that rises instantly to some value, $I_{o,}$ and maintains that value until just prior to the projectile exiting the barrel. Just before contact is lost with the projectile the current should then instantly fall to zero, as shown in Fig. 10, where *t* is equal to time.

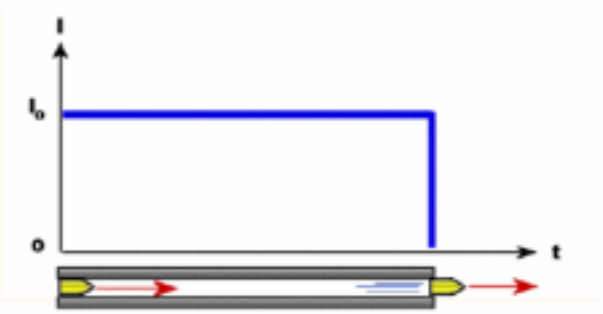

Figure 10. Ideal projectile current pulse. (From Ref. 6.)

Most experts involved in the development of railguns for shipboard application agree that there are currently only two technologies that are capable of meeting the power storage and delivery requirements for these systems. Those are capacitors and inertial-based power supplies, with each having their own advantages and disadvantages. It should be noted that due to the internal inductance associated with all systems and loads, it is impossible to instantaneously start or stop current flow, thereby making all systems less than ideal. The alternatives as they apply to the smaller research scale gun here at NPS will be examined in the following discussion.

1. Compensated Pulse Alternator

A compensated pulse alternator or "compulsator" is a single-phase or multiple-phase AC machine with a flux shield or compensating winding located in the air gap to lower or vary the machines impedance characteristic. There are three types of compensation: active, passive and selective-passive [9]. Active compensation places a stationary winding in the air gap that is nearly identical to the rotor winding and is connected in series with it. The result is that, as the rotor winding moves directly under the compensating winding, the full machine voltage is applied to the load without the compulsator impedance in the circuit. Active compensation results in a narrow pulse width current pulse that is very sensitive to the load inductance and is not suitable for railgun applications. In passive compensation machines the active windings are replaced by low impedance, continuously conducting shields with the compensation current being induced by the rotational field of the armature. The result is the compulsator impedance stays low for the full rotation of armature and the output waveform is a smooth sinusoidal shape with high peak currents. These machines have been used to power railguns, but the rapid sinusoidal rise and fall of the current pulse is not the ideal pulse shape. The most recent design used in railguns is the selective-passive compensation method. Unlike the passive method that uses an axis-symmetric shield, the compensating currents are constrained to flow in discrete short-circuited windings. This version allows the engineer to change the machine inductance characteristics based on the rotor position, thereby changing the output waveform [9].

The next step in the development of the compulsator is to move to a three-phase multi-pole machine to allow even greater flexibility in the control of the output current waveform. This represents the present state of the art in design and performance. Figure 11 is a cross-section view of a compulsator. Two of the drawbacks to using a single or multi-phase machine are that they operate at high RPM to maximize energy storage and require AC-to-DC conversion for the self-excitation current and the output current to the load, as shown in Fig. 12. In this schematic the full-wave rectifier converts the three-phase AC output to DC that powers the field windings while another set of thyristors

converts the output current to the gun. For the system at the University of Texas Austin Center for Electromechanics, the worst-case phase current requires 352 thyristors to build the converter for a 500-Hz system and 664 thyristors for a 2-kHz system [10].

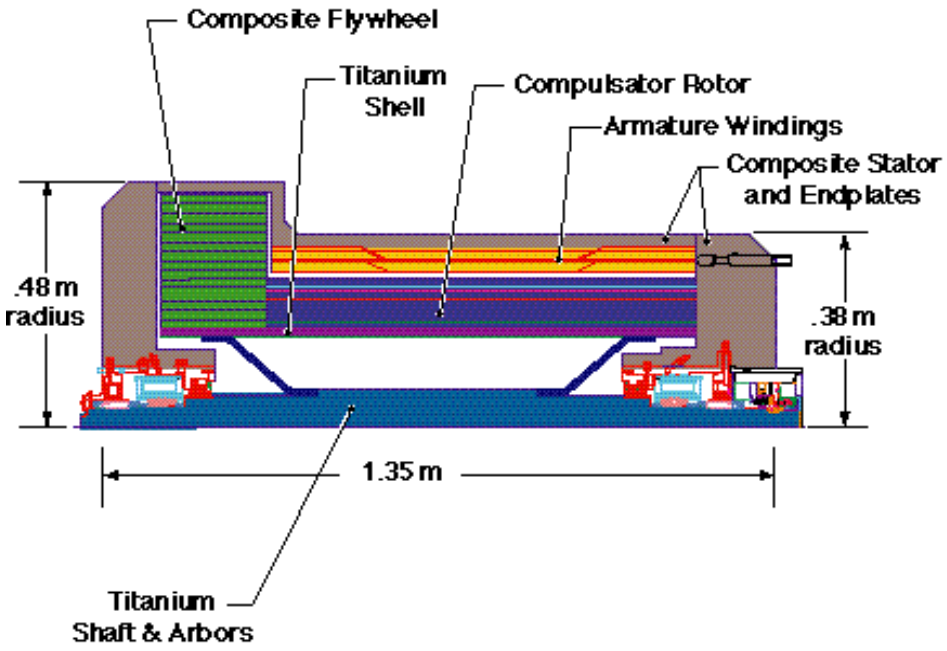

Figure 11. Cross-section view of a compulsator (From Ref. 8)

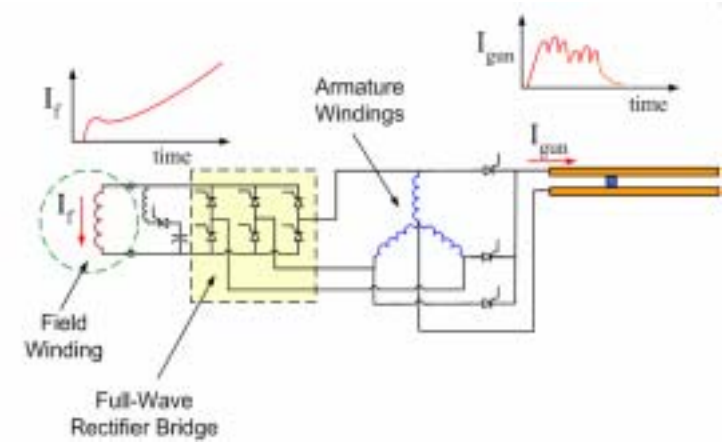

Figure 12. Compulsator simple circuit representation. (From Ref. 8.)

The problem with using a compulsator for this design is that they are not easily upgradeable. In order to improve the power output of the system, it would be necessary to buy an additional machine to replace or operate in parallel with the existing unit. Further, upgrading the converters to handle the increased current would be necessary. Additionally, compulsators are specialty items that have been designed and built for research, and are not available in the commercial marketplace. For those facilities that do use compulsators to power railguns, their research is focused more on the machine and less on the railgun itself.

2. Capacitor-based Systems

Capacitor-based systems are the most common type of pulsed power supplies used in railgun research. They usually consist of a number of individual capacitors grouped together and discharged simultaneously to form a module. These modules can then be grouped to form segments. The purpose of modules and segments is to provide a means of shaping the output pulse to provide a more constant current. By varying the inductance and capacitance values of a segment (the blue, green, red and light-blue traces in Fig. 13) and then sequentially discharging the segments it is possible to maintain a near constant output current (the magenta trace in Fig. 13) over a substantial part of the current pulse.

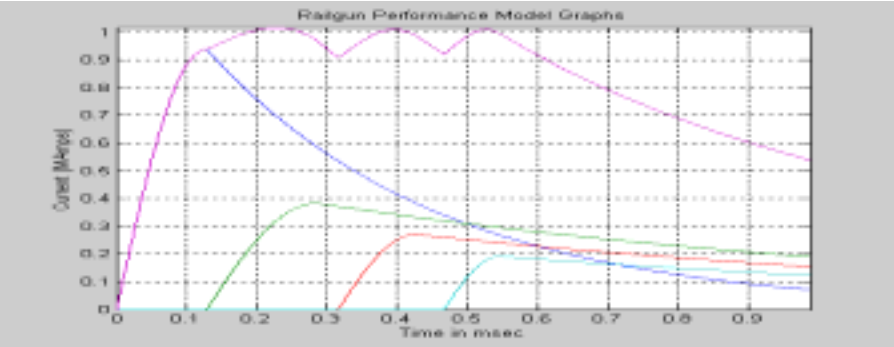

Figure 13. Output current waveform for a capacitor-based system.

The system itself is very simple and consists of the capacitors, pulse shaping inductors, the high power switches, the protection diodes for the capacitors, a charging power supply, and a trigger and control section for the switches. All of the components

have a proven performance record in the intended application and are commercially available. Additionally, a capacitor-based system can be upgraded by using a single capacitor or with an entire segment depending on the requirements.

3. Summary

Although compulsators show a promising future in full-scale production railguns, they are not a good option for the research being done here at the Naval Postgraduate School. The system is complex, expensive, experimental and immature as a technology. It is also not easily upgraded and not readily available for purchase. In contrast the necessary components for a capacitor-based system are mature as a technology and can easily be purchased once the system requirements are defined. Additionally, the lifetime maintenance costs for a capacitor-based system are expected to be less since there are no moving parts that require upkeep or replacement. In the event a capacitor fails, the system is still operable but at a slightly degraded capacity. Therefore, based on the resources and the intended application, the NPS pulsed power supply will be designed as a capacitor-based system. The following sections further explore the options for capacitor-based systems.

B. SINGLE CAPACITOR BANK MODEL

Capacitor-based systems can be described using a simple RLC circuit, as shown in Fig.14, where C is the system capacitance, L_o is system inductance, L_r is the variable inductance as the projectile moves down the barrel, and R is the system resistance.

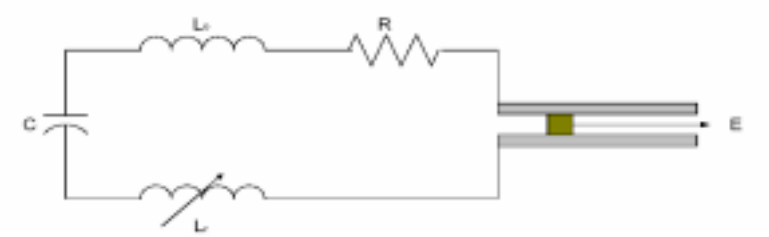

Figure 14. An ideal railgun circuit. (From Ref. 11.)

When the switch is closed in a capacitor-based pulsed-power supplies, the capacitor will begin to discharge into the system and transfer its energy into the inductor. At the point when the capacitor is completely discharged, the inductor will be fully charged and current will be at its peak. From this point the current will exponentially decay until the projectile exits the barrel resulting in an open circuit. Figure 15 shows a typical half-

period discharge cycle from the power supply for the Lockwood railgun in Fig. 6. This gun was designed as a 100-kJ gun and was powered by two 0.830-mF, 11-kV, 50-kJ capacitors.

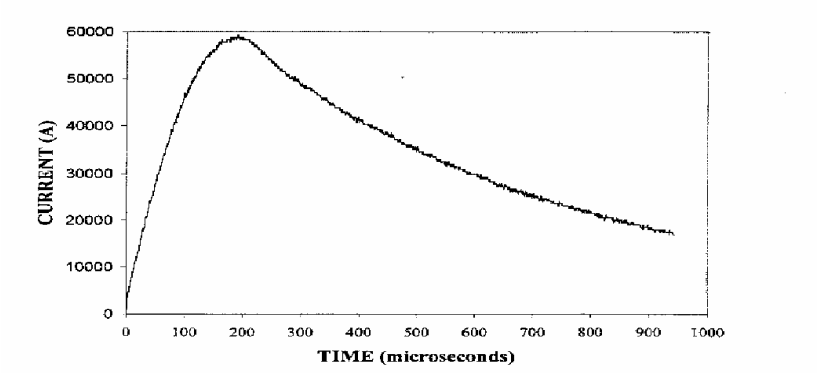

Figure 15. Lockwood 100 kJ power supply current waveform (From Ref. 7.)

The current rise can be closely approximated as a sine function

$$I = I_o \sin(\omega t), \tag{2.1}$$

and the current fall off can be described as

$$I = I_o e^{-\left(\frac{R}{L}\right)t}, \tag{2.2}$$

where $L = L_o + L_r$, $\omega = 1/\sqrt{LC}$, $I_0 = V_o\sqrt{C/L}$, and V_o is the initial capacitor voltage [6]. The MATLAB simulation results of the pulse in Fig. 16 are similar in form to Fig.15.

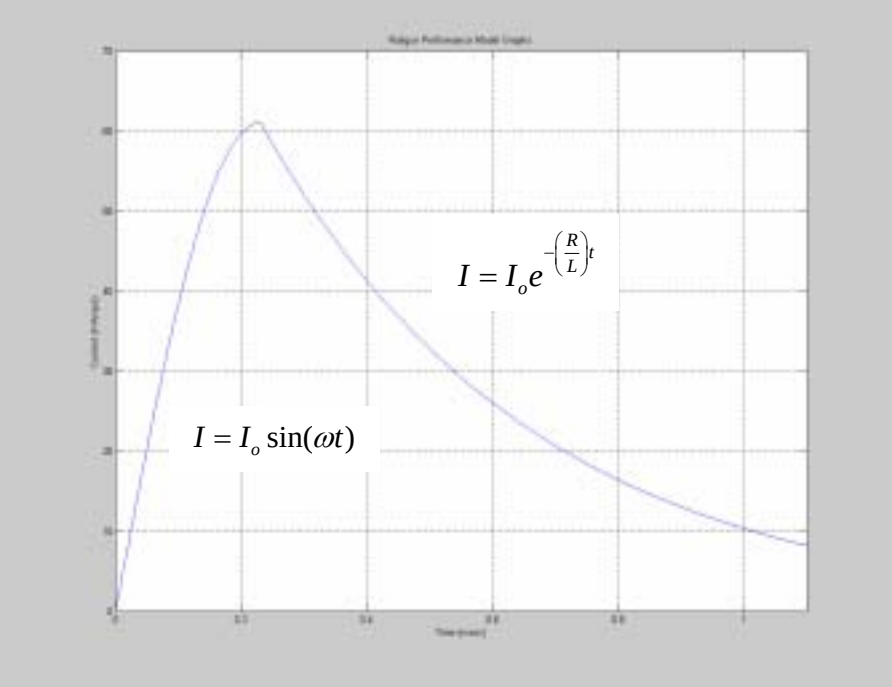

Figure 16. MATLAB model of the Lockwood gun current pulse.

By taking the model for the current pulse and applying it to Equation 1.10, it is possible to calculate the acceleration of the projectile at any time during the current pulse given the system parameters previously discussed. Substituting Equations 2.1 and 2.2 into Equation 1.10 results in the following expressions for acceleration:

$$a = \frac{1}{2m} L' \left(I_o \sin(\omega t) \right)^2 \quad \text{for } t < t' \tag{2.3}$$

and

$$a = \frac{1}{2m} L' \left(I_o e^{-\left(\frac{R}{L}\right)t} \right)^2 \quad \text{for } t > t', \tag{2.4}$$

where $t' = \pi\sqrt{LC}/2$, which corresponds to the time of the peak current value. This time also marks where capacitive discharge ends and inductive discharge begins. Dividing Equation 1.15 by the mass of the projectile and subtracting the results from Equations 2.3 and 2.4 will result in the final projectile acceleration. As stated earlier, once the acceleration is known, it is simply a matter of integration to calculate the velocity and position of the projectile. These equations were then programmed using MATLAB and included in

Appendix A. They will be used to conduct design trade-off studies between single and multi-bank PFN's. The multi-bank model will be discussed in the next section.

Appendix B contains a detailed discussion of how the values for the single-bank design were determined. The following is an explanation of the results for the purpose of comparing them to the multi-bank model. Table 4 summarizes the results of the analysis for the single-bank case. The term effective-barrel-length in Table 4 refers to the distance down the barrel where significant acceleration ends. This term is more thoroughly discussed in Appendix B. Figure 17 is the predicted current, acceleration, velocity, and displacement profiles from the MATLAB model. The green trace in the acceleration, velocity, and displacement graphs includes the effects of barrel friction, while the blue trace is the frictionless case.

Capacitance	21.58 mF	Muzzle Velocity	1002 m/s
Inductance	5.5 μH	Current Density	39.1 kA/cm^2
Resistance	0.003 Ω	Peak Current	626.4 kA
Voltage	10 kV	Exit Current	285.1 kA
Projectile Mass	171.5 g	Effective-barrel-length	0.82 m

Table 4. Single-Bank Performance Summary.

The selected system capacitance of 21.58 mF and inductance of 5.5 μH resulted in a predicted projectile velocity of 1002 m/s and a current density of 39.1 kA/cm^2, which are on the edge of the acceptable performance specification listed in Table 3. The important values to note from this analysis are the system peak current requirement of 626 kA (with a rise time of approximately 0.55 ms) and the current remaining in the barrel when the projectile exits of 285 kA.

The 626-kA peak current combined with the voltage hold-off requirement of 10 kV present a significant switching problem for this power supply configuration. The exit current is also significant in that it represents an energy loss that must be removed from the system in the form of heat, or recovered and fed back into the capacitor banks. Another detrimental effect caused by the exit current is related to the fact that this energy is

stored in the system inductance. As the projectile exits the barrel and contact is broken with the rails, the energy stored in the inductor causes a voltage spike in an attempt to maintain current flow. This voltage spike results in arcing between the muzzle and the projectile and is commonly referred to as “muzzle flash”.

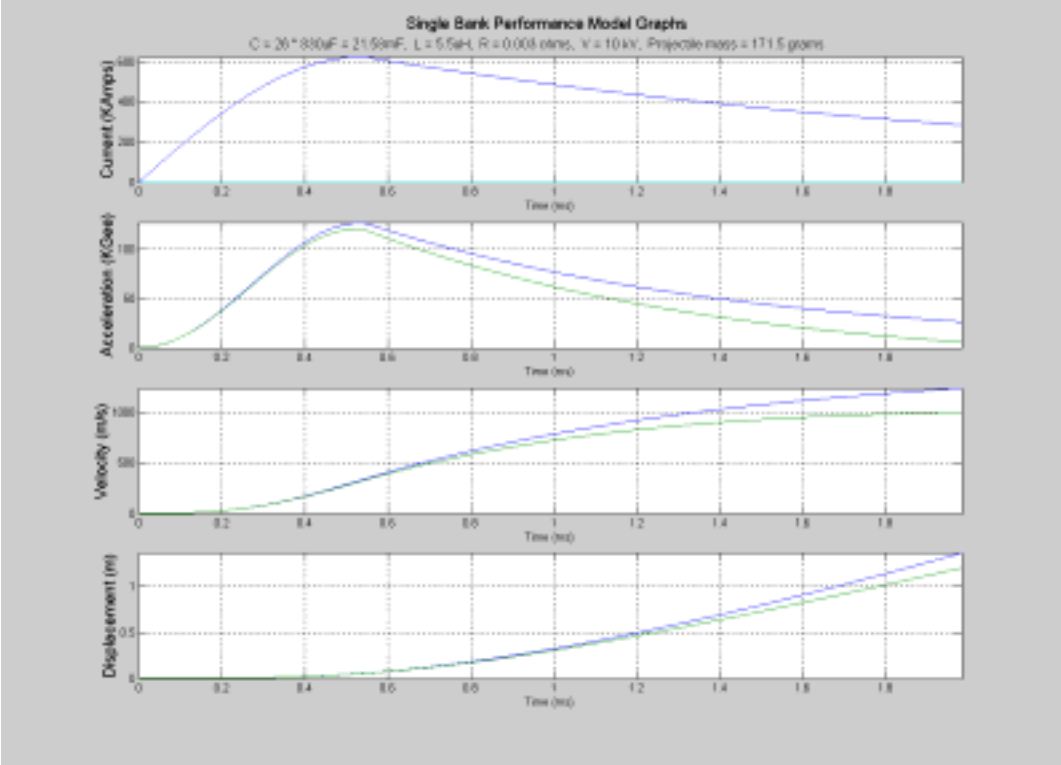

Figure 17. Single-bank performance model graphs vs. time.

While the capacitors store the energy and initiate the current pulse, the capacitive discharge phase does not provide the majority of the accelerating force to the projectile. Projectile acceleration occurs primarily in the inductive discharge phase, which is why it is important to maintain the peak current level high for as long as possible. A large system inductance could be used to extend the current pulse. Adding a large inductance would limit the peak current, require more capacitance in the power supply, and would increases the current in the barrel when the projectile exits. Decreasing the inductance to minimize the exit current is possible, but there is a minimum current that must be maintained to prevent the projectile from decelerating prior to exiting the barrel. To determine this value, it is necessary to know the frictional losses in the barrel. Assuming a 1000 m/s velocity and using the values listed Table 3, Equation 1.15 will determine the accel-

eration losses due to friction. Dividing Equation 1.15 by the mass of the projectile results in

$$a_{\text{friction}} = \frac{2vAu}{\Delta t(m)} = \frac{2 \times \frac{65\ \text{cP}}{1000} \times (0.1\ \text{m} \times .016\ \text{m}) \times 1000\ \text{m/s}}{0.171\ \text{g} \times 6 \times 10^{-6}\ \text{m}} = 202.8\ \text{kN}, \qquad (2.5)$$

where u is the velocity of the projectile and m is the mass of the projectile. Once the acceleration due to friction is known the required current to overcome friction can then be solved for in Equation 1.10:

$$I_{\text{friction}} = \sqrt{\frac{2ma_{\text{friction}}}{L'}} = \sqrt{\frac{2 \times 202.8\ \text{kN} \times 0.1715\ \text{kg}}{1.1\ \mu\text{H/m}}} = 251.5\ \text{kA}. \qquad (2.6)$$

When the projectile accelerates to 1000 m/s a current of 251.5 kA or greater must be maintained in the rails to prevent the loss of velocity due to friction. This point again emphasizes the importance of matching the power supply to the railgun. To use the barrel most effectively, the desired velocity should be reached just prior to exiting the muzzle. It is not necessarily detrimental to the overall performance of the gun if the barrel current decreases to less than I_{friction}, provided that this occurs near the end of the barrel. Smaller exit current can benefit the overall system design by reducing the barrel current when the projectile exits, thus reducing the muzzle flash. There are other methods of reducing the muzzle flash that will be discussed in a later section.

Figure 17 displays the results with respect to time, which does not always provide the clearest picture of what is occurring as the projectile travels down the barrel. A more useful way of viewing this information is with respect to barrel length or displacement, as shown in Fig. 18. From this perspective the need to match the railgun to its power supply is very apparent. The velocity graph in Fig. 18 shows that the projectile gains 80% of its speed in the first 33% of the barrel. This implies that the heating and erosion effects will be the greatest in this region. The current profile also shows that the projectile moves very little as the current rises to its peak value of 626 kA, which further complicate the rail erosion problems.

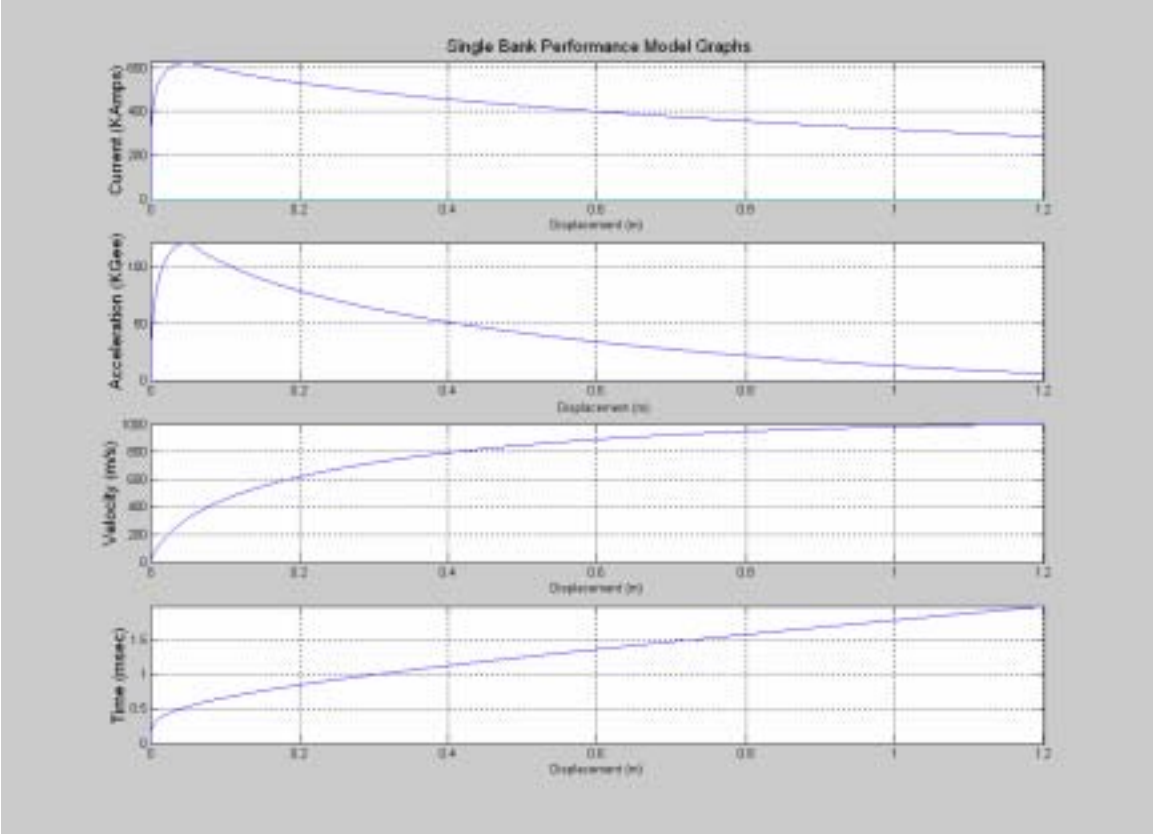

Figure 18. Single-bank performance model graphs vs. displacement.

The strength of the single-bank system is that it is simple and easily controlled with a single switch or set of switches fired simultaneously to produce one pulse. The disadvantages are a high switch current requirement for the peak system value, a high exit current requirement for efficient barrel use, and a large capacitance requirement. The multiple-bank model discussed next provides solutions to some of these problems.

C. MULTIPLE CAPACITOR BANK MODEL

The multiple-bank model can be constructed by the superposition of single-bank models with an appropriate time delay inserted between bank discharges. The current pulse in Fig. 13 is an example of this model. For analysis purposes our model will include four equal banks of capacitors fired at the peak current level of the previous bank. Table 5 contains a list of assumption used for the multiple-bank trade-off studies.

Barrel length: 1.2 m	Bore height: 1.6 cm	Bore width: 1.6 cm
Minimum Inductance: 2.5 μH	Resistance: 0.003 Ω	L' based on Eq. 1.13: 1.1 μH/m
Voltage: 10 kV	Projectile Density: 6.7 g/cm^3	Projectile weight: 171.5 g
Projectile Length: 10 cm	Silver paste viscosity: 65 cP	Maximum projectile current density: 40 kA/cm^2

Table 5. Assumptions for the multiple trade-off studies.

The following list of objectives was used to conduct trade-off studies to produce the final results of the multiple-bank model:

1. Minimize the capacitance to meet the desired muzzle velocity.
2. Minimize the barrel current when the projectile exits.
3. Optimize the current pulse to maximize the barrel usage.
4. Maintain the projectile current density as low as possible.

In order to optimize the barrel usage it is necessary to produce a flatter pulse than the one shown in Fig. 16. The parameters that control the pulse shape are L, C, R and the delay between pulses. The resistance term is an intrinsic value of the system, it cannot be easily decreased, and it is undesirable to increase it. For this reason the resistance will be treated as a constant. An increase in inductance will cause the desired effect of reducing the peak current and slowing the inductive phase current falloff. Increasing the inductance will have the positive effects of reducing the current density while lengthening the pulse to more closely match the barrel length, but will results in a higher barrel current when the projectile exits. Another way to increase the barrel usage in the multiple-bank case is to increase the delay time between bank discharges. Delaying the bank discharges results in lower peak currents and higher effective-barrel-lengths. Because acceleration is proportional to the current squared, the average acceleration is lower for the increased inductance case and subsequently causes the muzzle velocity to also be lower. In order to compensate for the loss in velocity it is necessary to increase the amount of capacitance in the power supply, assuming a constant voltage. Increasing the capacitance is in con-

flict with the stated objective to minimize the capacitance, and also results in an increased peak current and a current density that may be higher than in the lower inductance case.

From the above discussion it is clear that designing a power supply for a railgun is an exercise in system optimization. In order to identify the design space for the multiple-bank model, plots of muzzle velocity, muzzle current, current density, and effective-barrel-length versus inductance and capacitance were constructed. These plots were then used to estimate the size of the capacitor banks and system inductances. The estimates were then put back into the multiple-bank performance model for further refinement and analysis.

The two most important aspects of the design are meeting the minimum muzzle velocity of 1000 m/s and the maximum projectile current density of 40 kA/cm^2. The acceptable combinations of capacitance and inductance that will meet the velocity requirement is any combination on or above the 1000 m/s contour line in Fig. 19. The area above the 1000 m/s contour is referred to as the velocity design space. Similarly, any combination of capacitance and inductance below the 40 kA/cm^2 contour in Fig. 20 will result in an acceptable current density. The area above the 1000 m/s contour is referred to as the current density space.

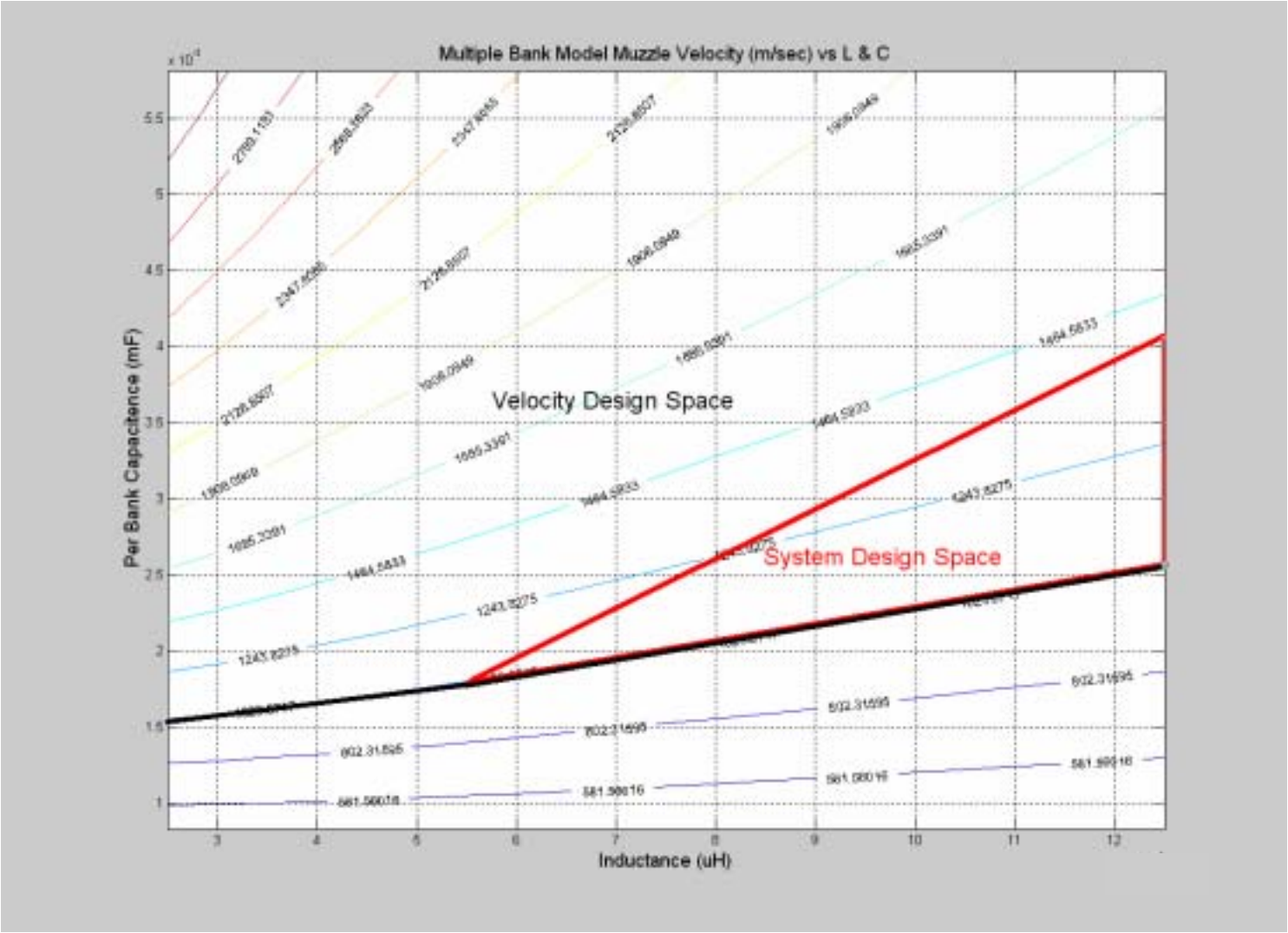

Figure 19. Multiple-bank muzzle velocity contour plots and system design space.

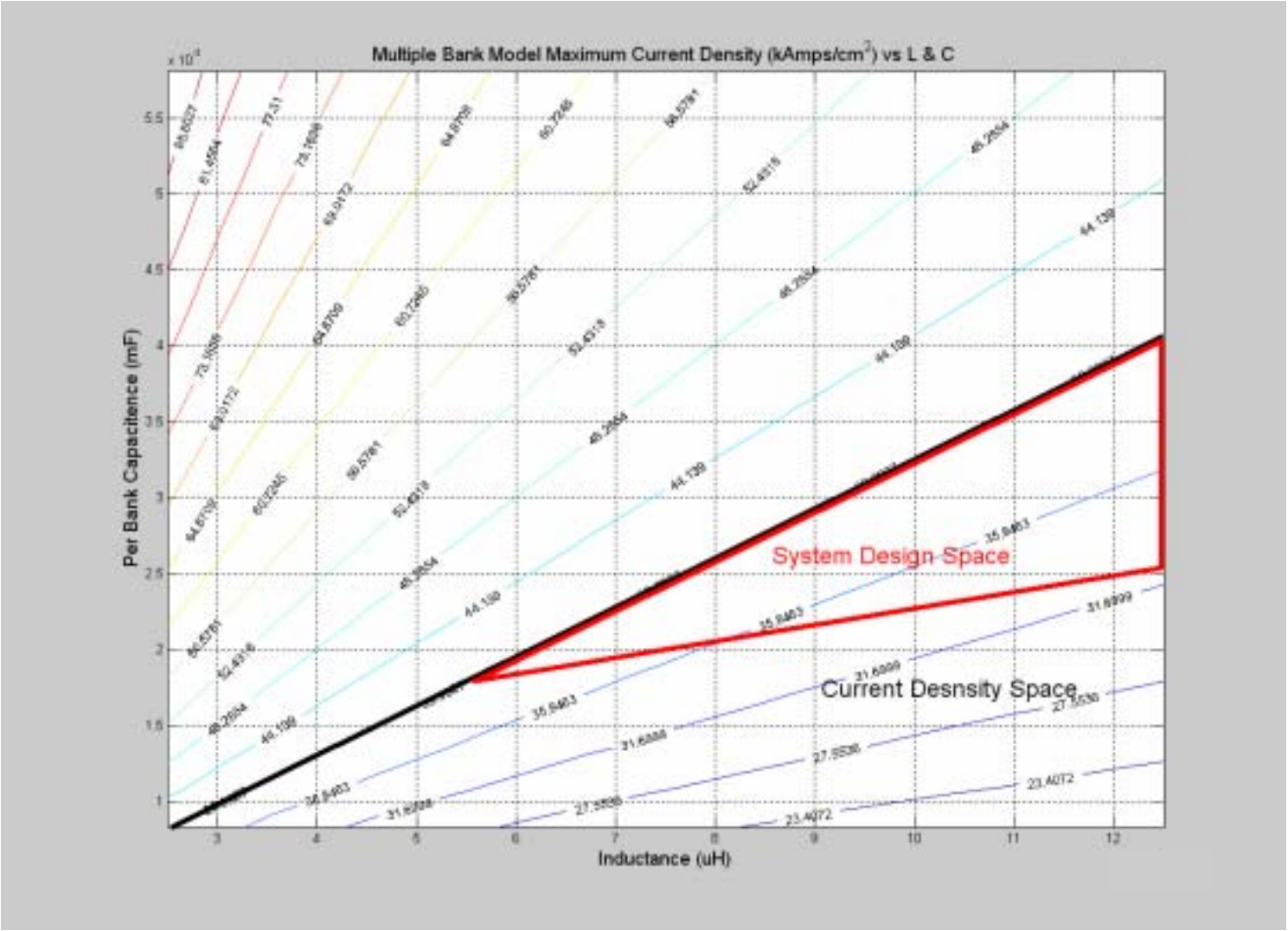

Figure 20. Multiple-bank maximum current density plots and system design space.

The lowest capacitance in the design space is 1.5 mF per bank and 6 mF total. It is not surprising that the lowest capacitance capable of providing 1000 m/s corresponds to the minimum inductance value of 2.5 μH. Note that the firing delays associated with the multiple-bank model have reduced the system capacitance a factor of three compared to the single-bank case. It is also important to point out that in the interest of minimizing the capacitance and thus the system cost, the final design point should be as close to the 1000 m/s contour as practical.

As expected when the inductance goes up, the current density decreases for a given capacitance since the peak current value is decreased. The overlapping area between the velocity design space and current density design space is considered the system design space. Any combination of capacitance and inductance that falls inside the red triangle areas in Fig. 19 and Fig. 20 will result in a design that meets the two previously stated design requirements.

The next step is to attempt to optimize the system to maximize the effective-barrel-length and minimize the muzzle current while staying inside the system design space. To do this it is necessary to explore the design space as it relates to the effective-barrel-length and muzzle current contour plots of Fig. 21 and Fig. 22, respectively. Again, there is a conflict between minimizing the capacitance while optimizing the effective-barrel-length and muzzle current. The lower left corner of the design space triangle represents the best possible solution for minimizing capacitance and muzzle current, but is the worst case for effective-barrel-length and current density. The lower right corner represents the best-case current density solution, but is sub-optimal for capacitance, barrel length and muzzle current. The upper right corner is the worst-case solution for capacitance, muzzle current, and current density, but it does provide the maximum use of the barrel. The overriding concern is the cost of the system, which is dominated by the cost of the capacitors. It is for this reason that solutions near the lower left corner will be preferred over solutions in the upper right corner.

The General Atomics (GA), Series C, 830-μF, 11-kV capacitor was chosen as the reference capacitor for use in this design [12]. To meet the minimum acceptable

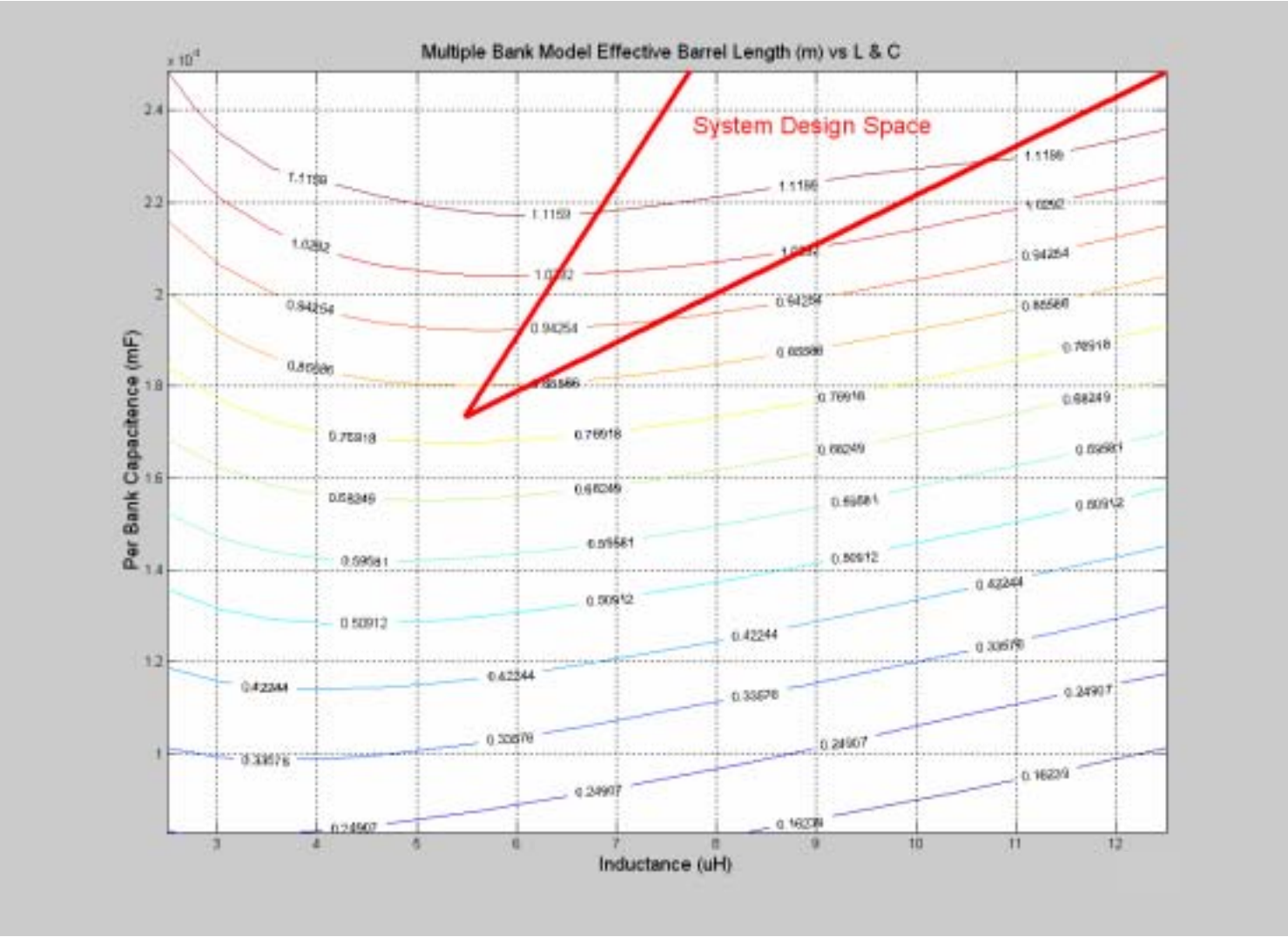

Figure 21. Multiple-bank effective-barrel-length contour plots.

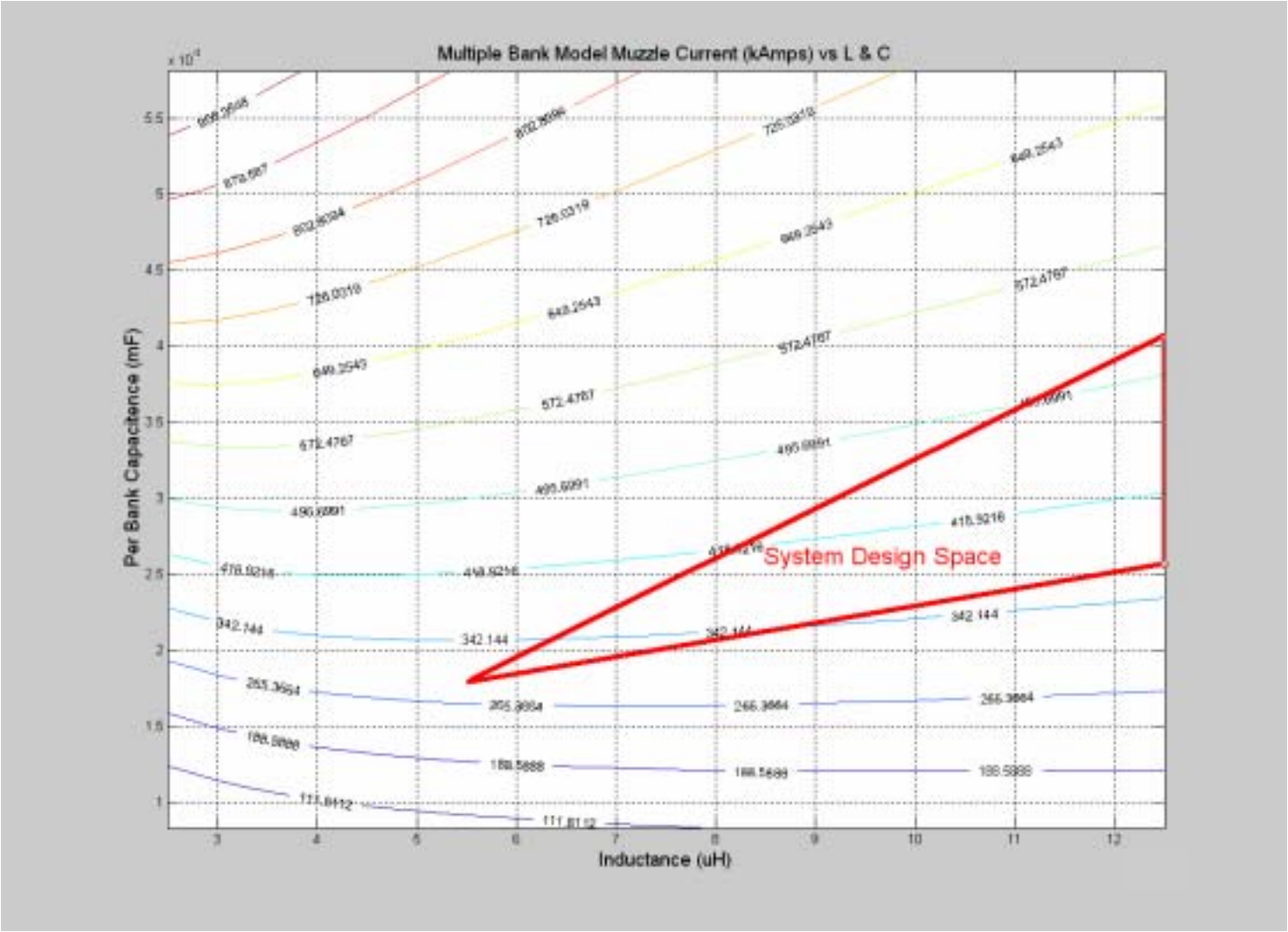

Figure 22. Multiple-bank muzzle current contour plots.

capacitance and remain in the design space will require three capacitors per bank and 12 capacitors for the system resulting in a total bank capacitance of 9.96 mF. This capacitance corresponds to inductance values in the range of 7.7 μH to 12 μH. The actual minimum capacitance per bank is 1.75 mF which is slightly greater than two of the above-mentioned capacitors. In order to meet the requirement it was necessary to use three capacitors per bank resulting in an over designed system.

Because the power supply is over designed with respect to capacitance, the effective-barrel-length from Fig. 21 is greater than 1.12 m for all values of inductance corresponding to 2.49 mF in the design space. This implies that the system inductance should be chosen to minimize the exit current without regard to its impact on effective-barrel-length. Following this logic leads to an inductance of approximately 7.7 μH. Table 6 is a summary of the multiple-bank model outputs, and Fig. 23 is the current, acceleration, velocity, and displacement profiles for the model. As in the single-bank plots of Fig. 17, the green trace includes the effects of friction and the blue traces are the frictionless case.

Capacitance	9.96 mF	Muzzle Velocity	1213 m/s
Inductance	7.7 μH	Current Density	39.9 kA/cm^2
Resistance	0.003 Ω	Peak Current	637.9 kA
Voltage	10 kV	Exit Current	398.8 kA
Projectile Mass	171.5 g	Effective-barrel-length	1.2 m

Table 6. Multiple-bank zero time delay performance summary.

The primary difference between these graphs and the single-bank model graphs is the time at which the peak current and acceleration occurs. For the single-bank case these peaks occurred at 0.55 ms and for the multiple-bank case they occurred at approximately 0.85 ms. For both the single and multiple-bank cases, the current and acceleration peaks are of similar value with the major difference being the time the peak occurs. Because the peak occurs later in the multiple-bank case, there is less time for the pulse to decay. The delay in the peak current is compounded by higher system inductance than in

the single-bank case slowing the current to fall off. This results in a higher effective-barrel-length at the expense of a higher exit current.

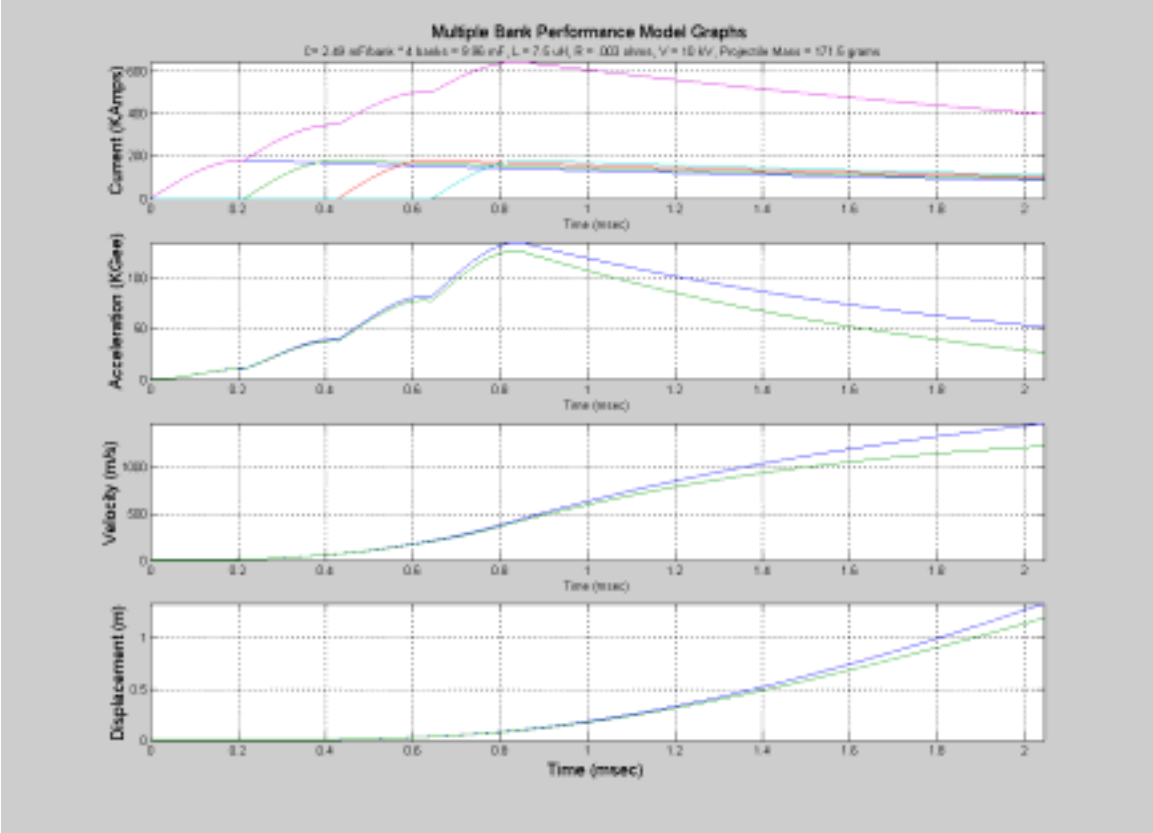

Figure 23. Multiple-bank performance model graphs vs. time.

Other than the obvious reduction in system capacitance and the increase in muzzle velocity to 1213 m/s, there does not appear to be a great advantage in the multiple-bank case over the single-bank case. By lowering the bank voltage the peak current and current density can be lowered. Doing this results in the muzzle velocity and the effective-barrel-length decreasing. Even though the effective-barrel-length is shortened because the system is operating at a lower peak current density, the life expectancy of the rail should be improved. Table 7 shows the effects on performance of decreasing the bank voltage to 8.9 kV.

The multiple-bank model is an improvement over every aspect of the single-bank model, except exit current. There are three options remaining that can be used to further shape the pulse and improve the exit current. Unlike the single-bank model where the

pulse shaping inductance is lumped into a single inductor, the multiple-bank model inductance can be varied on a per bank basis. By decreasing the inductance of the later

Capacitance	9.96 mF	Muzzle Velocity	1002 m/s
Inductance	7.7 μH	Current Density	35.5 kA/cm^2
Resistance	0.003 Ω	Peak Current	567.8 kA
Voltage	8.9 kV	Exit Current	321.5 kA
Projectile Mass	171.5 g	Effective-barrel-length	0.96 m

Table 7. Multiple low voltage performance summary

firing banks, the current can fall off faster resulting in a lower exit current. Another possibility that has yet to be addressed is the time delay between bank firings. Until now all modeling has been done with each bank firing at a time corresponding to the peak current of the previous bank. By delaying the firing times it is possible to lower the total peak current and increase the effective-barrel-length. It is also possible to shape the pulse by implementing a non-uniform capacitance distribution among banks. The most effective implementation would be to place a large percentage of the system capacitance in the first bank and then use the following banks to boost the current as necessary.

Table 8 lists the system capacitance, inductance and time delays for the multi-variable case. Bank one capacitance value is 7.47 mF that corresponds to nine GA 0.830-mF capacitors, while banks two, three, and four each contained one capacitor. The total capacitance is equal to 9.96 mF as in the previous multiple-bank cases, and all capacitors were charged to 10 kV. The bank inductance (for banks two and three) is 2.5 μH based on the assumed minimum system inductance. All time delays are measured from the peak of the previous current pulse.

Table 9 is the multi-variable performance summary. The primary increase in performance is in the area of exit current, but at the cost of effective-barrel-length. It should be emphasized that not all the possible combinations of capacitance, inductance, and time

delays were examined due to the magnitude of such an undertaking, so a combination yielding better performance may exist.

	Capacitance	Inductance	Time delay
Bank 1	7.47 mF	4.5 μH	N/A
Bank 2	0.83 mF	3.5 μH	0 ms
Bank 3	0.83 mF	2.5 μH	0.4 ms
Bank 4	0.83 mF	2.5 μH	0.4 ms

Table 8. Multiple-bank multi-variable system values.

Capacitance	See Table 8	Muzzle Velocity	1006 m/s
Inductance	See Table 8	Current Density	35.4 kA/cm^2
Resistance	0.003 Ω	Peak Current	566.6 kA
Voltage	10 kV	Exit Current	262.2 kA
Projectile Mass	171.5 g	Effective-barrel-length	0.88 m

Table 9. Multiple-bank multi-variable performance summary.

Figure 24 is the current, acceleration and velocity profiles from the multi-variable case. The most obvious and important difference between this case and the previous cases are the three distinct current pulses with peak values greater 560 kA. The peak current density of 566 kA is the lowest of the four cases examined, but does not convey the complete picture. In the three previous cases the project was subjected to the peak current and peak current density only once per shot. For this case the projectile and rails will have to withstand the peak current density condition three times, which may prove to be more taxing than a single occurrence at a higher current density.

The best overall predicted performance comes from the multi-variable case, but may not be the best solution. It is also less flexible with regard to changes in voltage.

Since the low voltage case is operated 1100 V below the other options, it has greater flexibility in compensating for estimation errors in the model. The multiple-bank (low voltage) case provides nearly identical performance to the multi-variable case. The exceptions are effective-barrel-length and exit current. Table 10 is a summary of the four previously discussed design cases.

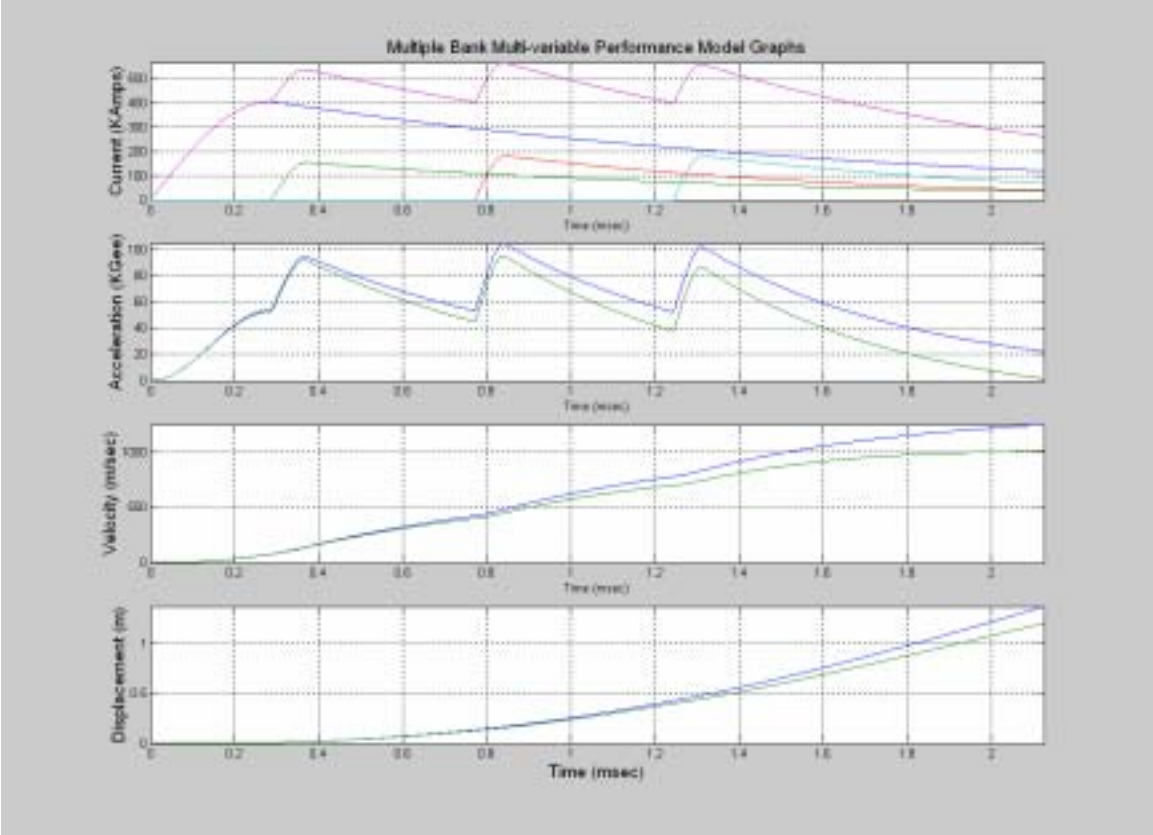

Figure 24. Multiple-bank Multi-variable performance model graphs.

The final design will be based on the multiple-bank (low voltage) case for the following reasons:

1. The switch requirements are less demanding than in the single-bank case due to the current being equally shared by the four banks.
2. The switch hold-off voltage requirement is less than in the other cases, which further reduces the switching requirements.

3. The pulse shaping inductance is a single value for all banks and can be placed in series between the capacitor banks and the railgun. This ensures that all banks see the same load impedance.
4. All banks are triggered with the same time delay reducing the need for individually adjustable timing circuits.
5. Because the capacitors will be operated 2100 V below the rated voltage, there is a larger margin for error. The capacitor life is also extended.

	Single-bank	**Multiple-bank**	**Multiple-bank (Low Voltage)**	**Multiple-bank (Multi-variable)**
Capacitance	21.58 mF	9.96 mF	9.96 mF	9.96 mF
Voltage	10 kV	10 kV	8.9 kV	10 kV
Muzzle Velocity	1002 m/s	1213 m/s	1002 m/s	1006 m/s
Current Density	39.1 kA/cm^2	39.9 kA/cm^2	35.5 kA/cm^2	35.4 kA/cm^2
Peak Current	626.4 kA	637.9 kA	567.8 kA	566.6 kA
Exit Current	285.1 kA	398.8 kA	321.5 kA	262.2 kA
Effective-barrel-length	0.82 m	1.2 m	0.96 m	0.88 m

Green indicated the best performance and red indicates the worst performance in an area

Table 10. Design performance summary.

The only disadvantage to choosing this configuration is the high muzzle exit current. This current was not viewed as a major disadvantage, because the best-case scenario for a 1000 m/s projectile was 251.5 kA from Equation 2.6. Since the overall system will include a muzzle shunt to reduce the "muzzle flash" and barrel damage, the higher exit current is acceptable under these conditions.

By taking a systematic approach and defining a design space for both the single and multiple-bank scenarios, four possible configurations were identified and modeled. The multiple-bank (low voltage) case provides the best overall performance, and has lower peak currents per bank and a lower system operating voltage. The lower peak currents per bank and operating voltage reduce the switching and cabling requirements, thereby reducing the total system cost. Now that the power supply configuration and performance parameters have been established, it is possible to research the available components to meet these requirements. The next chapter will discuss the various components of the PFN in detail and give a recommended design and parts list based on the multiple-bank (low voltage) performance model.

THIS PAGE INTENTIONALLY LEFT BLANK

III. POWER SUPPLY DESIGN

In this chapter some of the primary components necessary to build this power supply design will be discussed. There are many other smaller circuits and parts that will be required to make the overall system fully operational, such as timing and control circuits for the bank isolation switches and fuses to protect the capacitors. These items are important to the design and its safe operation, but will not be discussed in this or the following chapter, as they are not the primary focus of this thesis.

A. CAPACITORS

The capacitors chosen for this design are the GA, 830-μF, 11-kV, 50-kJ, series C. These were preferred over other types of capacitors because they are readily available and NPS currently possesses a number of them. They are not cutting edge capacitor technology with respect to power density, but are capable of meeting the power and space requirements for this design while having a proven history in railgun applications. Table 11 is the technical specification for the GA, Series C, model 32327 capacitor.

The anticipated volume for the capacitors in this power supply is 36.7 ft^3 based on the case size and the required number of capacitors (12). An additional factor of 150% must be added to account for maintenance access, bank isolation switches, and other various components associated with the power supply and results in a required space of 91.8 ft^3. Assuming that the modules can be stacked two banks high with 24″ of separation between them, the required floor space would be 20 ft^2.

Capacitance	830 μF	Inductance	< 40 nH
Energy	50 kJ	Case size (LxWxH)	12x16x27.5
Max Voltage	11 kV	Design Life (100% voltage)	3000 shots
Voltage Reversal	10%	Weight	320 lbs
Peak Current	150 kA	Operating Temperature	25°C

Table 11. General Atomics, Series C, model 32327 technical data. (After Ref.12.)

All four banks are identically configured; therefore, the current pulse from each bank will also be identical, as seen in Fig. 23. The predicted peak current from each bank is 160 kA. Each bank will have a total of three capacitors in parallel resulting in a peak current per capacitor of 53.3 kA, which is well below its rated peak current of 150 kA. The power supply will also be operated at 8.9 kV or 81% of its 11-kV voltage rating. The combination of operating below both the rated current and voltage will provide a safety margin to prevent catastrophic failure of the capacitors and will extend their life. Not all the shots from this gun will require the capacitor banks to be charged to full rated voltage. Assuming that the average charge voltage per shot is 65% of the rated capacitor voltage and using the Charge Voltage Coefficient-of-Life Curve in Ref. 12, the life expectancy multiplier is 20 and equates to 60,000 charge/discharge cycles or shots.

The life expectancy could be shortened if the banks are allowed to exceed the 10% voltage reversal limit. Reference 12 also provides a Voltage Reversal Coefficient-of-Life Curve to estimate the effect of exceeding 10% voltage reversal on the design life. Allowing the voltage reversal to increase to 25% of the rated voltage would result in a 50% reduction in design life. For this reason every effort will be made to limit the voltage reversal to less than 10% of the rated voltage. Operating temperature can also reduce the design life of the capacitors. Increasing the operating temperature from 25°C to 35°C will cause the design life to be reduced by 50% [12].

B. SWITCHES

The switches represent the seconded largest cost of the system. Many of the decisions made in the previous chapter were to reduce the number of switches required in an attempt to minimize the cost of the system. Dividing the banks equally, as previously discussed, reduced the peak currents that each switch would be required to handle. An additional benefit of dividing the banks is that the hold-off voltage can be reduced from 10 kV to 8.9 kV. To provide a safety margin, 10 kV will be used as the design hold-off voltage. The current rise time is also a consideration when selecting switches for pulsed power systems. In this design the pulse rise time per bank is approximately $1.0\ \mathrm{kA/\mu s}$. In order to provide a safety margin and allow for future system growth, a pulse rise time of $2.0\ \mathrm{kA/\mu s}$ will be assumed. For vacuum or spark-gap switches it is necessary to know

the amount of charge transferred through the switch. Since $Q = CV$, the charge per bank will be equal to $2.49\ \text{mF} \times 10\ \text{kV} = 24.9\ \text{C}$. Table 12 summarizes the switch requirements for this design.

Hold-off Voltage	10 kV
Peak current	200 kA
Current rise time	2.0 kA/μs
Charge Transfer	24.9 coulombs

Table 12. Summary of switch requirements.

The two primary candidates for switches are solid-state and spark-gap switches. The two leading manufactures for these types of switches are Silicon Power Corporation (SPCO) in Exton, PA and Titan Corporation, Pulsed Science Division in San Leandro, CA, respectfully. Each switch has its own distinct advantages and disadvantages that will be discussed in the following sections.

1. Spark-gap

Spark-gap switches work by using a large trigger voltage to establish a plasma arc between a set of electrodes. Once this arc is established a current path is formed between the electrodes and remains until the current level decreases to the point that the plasma field can no longer be maintained. Figure 25 shows a typical electrode arrangement for a spark-gap switch. The Titan Corporation's ST-300A spark-gap switch shown in Fig. 26 is a two electrode dry air dielectric switch with a voltage rating of 0–55 kV. It is capable of handling peak currents in excess of 600 kA and transferring as much as 540 C per shot. The expected electrode life is 160 kC of total charge transfer, which equates to approximately 6400 full power shots from this power supply. Once the electrode life has been exceeded, it is possible to replace the electrode and restore the switch to full operation [14].

The advantages of using a spark-gap switch are the high peak current rating, hold-off voltage, and the ability to replace the electrodes. Because each switch has a rated hold-off voltage up to 55 kV and peak current rating of 600 kA, the power supply could be expanded to 40 capacitors per bank without exceeded the current or charge transfer limits of the switch. Because the ST-300A has a high peak current rating only one switch per bank will be required.

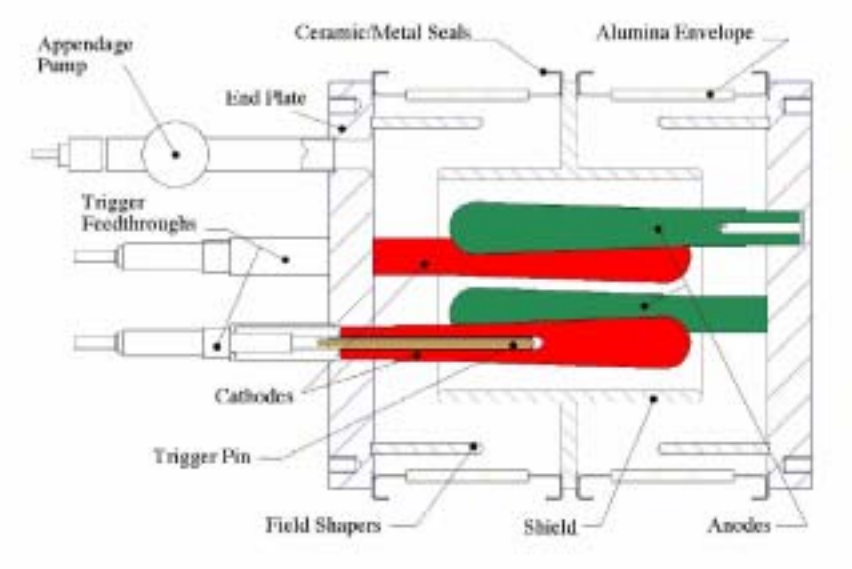

Figure 25. Cross section view of a spark-gap switch. (From Ref 13.)

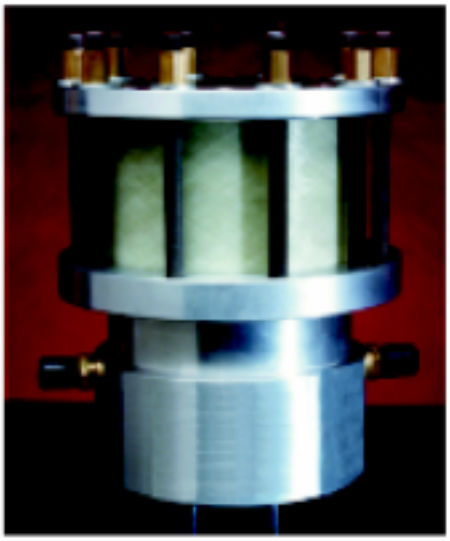

Figure 26. Titan Corporation ST-300A Spark Gap Switch. (From Ref. 14.)

The disadvantages of the ST-300A include size, weight and cost. The switch is 11.5″ tall with a 9″ diameter and weighs over 30 lbs. The cost of each switch is $3,880 plus $8,300 for the trigger generator (TG-75), also sold by Titan Corporation. The total cost for all four system switches would be $48,720. Two other disadvantages of the spark-gap switches are higher voltage drops after commutation compared with solid-state switches and high voltage triggers. Figure 27 shows that the voltage drop across a typical spark-gap switch is between 50 V and 150 V. (It should be noted that Fig. 27 is not specific to the ST-300A and was produced for a 225 kA peak current pulse, which is larger than the predicted current pulse for this design.) The recommended trigger pulse is twice the bank voltage for 50 ns to minimize the commutation losses.

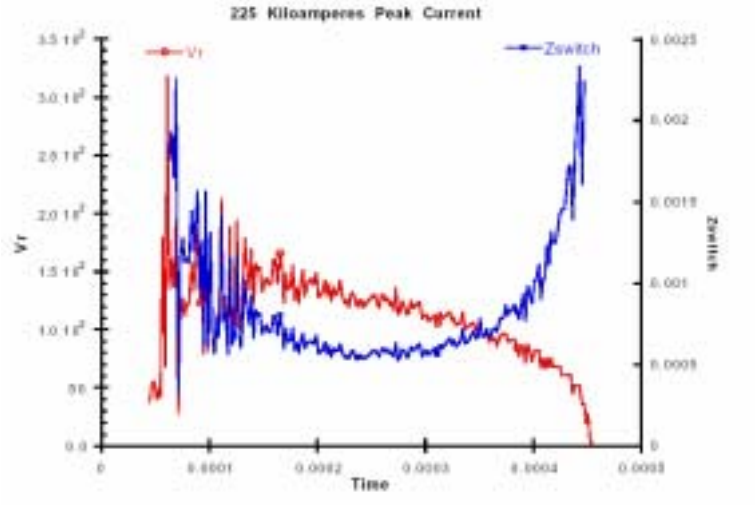

Figure 27. Spark-gap switch voltage and resistance curves. (From Ref. 13.)

2. Solid State

The SPT-411A is a solid-state switch that is part of the thyristor family and behaves similar to a Silicon Controlled Rectifier (SCR). Once the device is triggered, it will to conduct until the current flow stops or attempts to reverse. SPCO's SPT-411A is the primary thyristor candidate for this design. The SPT-411A is a 125 mm Light Silicon Sandwich (LSS) switch. The switch is constructed using a silicon layer separated by alloy-tungsten-alloy layers and mounted on a silicon substrate, as depicted in Fig. 28. It should be noted the LSS design is exclusive to SPCO's devices. The primary advantage of the LSS over conventional designs is its improved thermal conductivity. By fabricating the switches in this manner it is possible to achieve very high current densities

through the device while minimizing the size and weight. The LSS configuration combined with the highly "interdigitated" gate-structure shown in Fig. 29 enables the SPT-411A to handle current pulses up to 147 kA for 1.5 ms with a voltage hold-off of 5 kV [16].

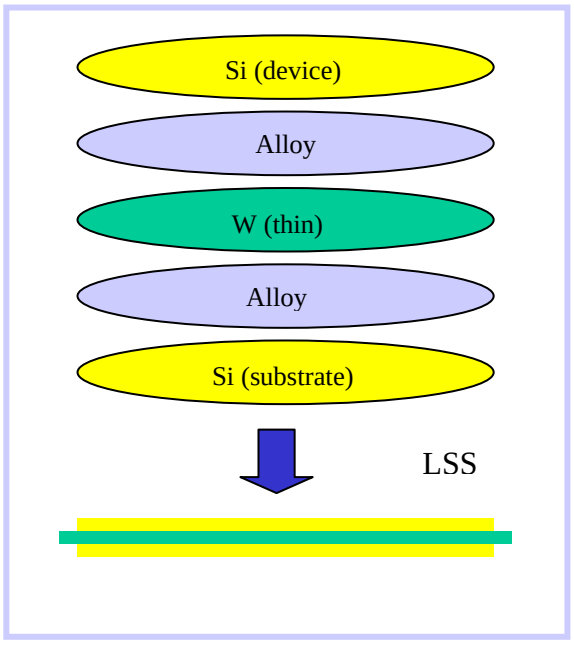

Figure 28. Silicon Power LSS design layers. (From Ref. 15.)

Figure 29. Silicon Power interdigitated gate structure. (From Ref. 15.)

Because the SPT-411A would be operating near or slightly over its peak half-cycle current rating it was necessary to more closely investigate the switch's characteristics in order to determine the exact number required for this application. Since the voltage hold-off rating for the switch is only 5 kV, it will require a set of two devices in series to achieve a 10-kV voltage rating and meet the 8.9-kV system requirement. The question that must be answered is whether it will require a single set of switches or two sets in parallel. The primary factor of concern is heat generation in the device. In order to determine the heating of the device, a data file containing the estimated current pulse for a single bank was given to Todd Hansen at SPCO. He then used a simulation program developed by SPCO to model the switch performance under our predicted conditions. Figure 30 is the SPT-411A single set temperature profile. The green trace is the estimated current pulse for a single-bank from the multiple-bank model, and the blue trace is the predicted temperature profile for the SPT-411A for the single bank current pulse. The initial ambient temperature of the device at the start of the simulation is assumed to be 30°C. Once the simulation is started the temperature of the device rises to a peak of 390°C at 4 ms. This temperature is outside the SPt-411A's operating range and would result in a catastrophic failure. These results indicated that there must be at least two parallel stacks of two devices.

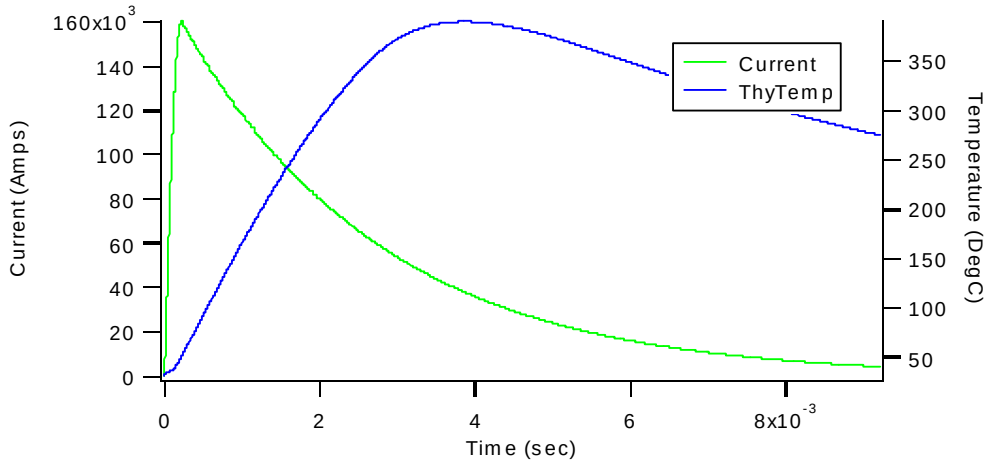

Figure 30. SPT-411A single stack temperature profile. (From Ref 17.)

In order to confirm that two parallel stacks would be adequate for the given current pulse, the simulation was repeated with a current pulse of half the peak amplitude of

the previous simulation. Figure 31 is the SPT-411A parallel set temperature profile. As in Fig. 30, the green trace is the input current pulse and the blue trace is the temperature profile. The initial conditions are the same as in the single set case, but resulted in a temperature peak of 82.5°C at 3 ms. This temperature is within the operational capability of the device. Assuming that the switches are allowed to cool to 30°C between shots, the estimated lifetime of the devices is 6 million shoots.

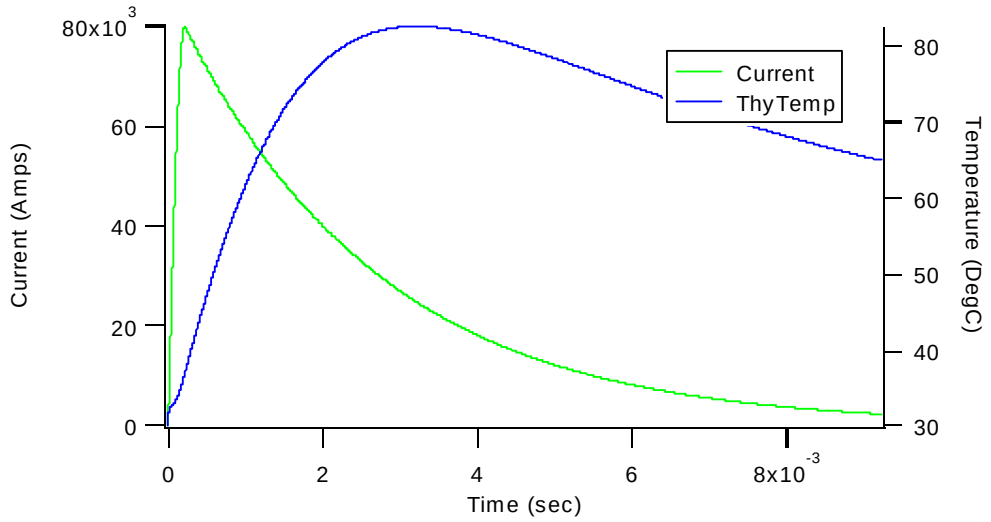

Figure 31. SPT-411A Parallel Set temperature profile. (From Ref. 15.)

These devices are non-linear in nature especially when operated under pulsed conditions. Figures 32 and 33 were provided by SPCO and show the resistance and voltage drop of the SPT-411A with respect to time for a 160 kA current pulse. Figure 32 shows that once commutation is complete and the switch is conducting, the resistance varies between 47 μΩ and 73 μΩ. The increase in resistance is due primarily to the temperature effect in the device. The voltage curve of Fig. 33 exhibits the opposite trend after commutation and more closely follows the current waveform. The voltage drop across the device does not fall-off as fast as the current due to the increasing resistance.

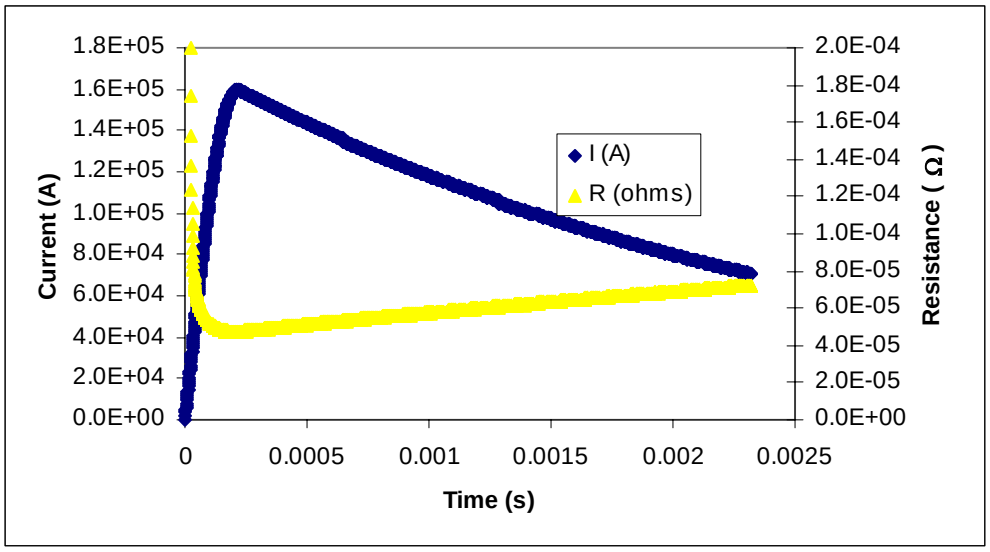

Figure 32. SPT-411A conducting resistance versus time. (From Ref. 15.)

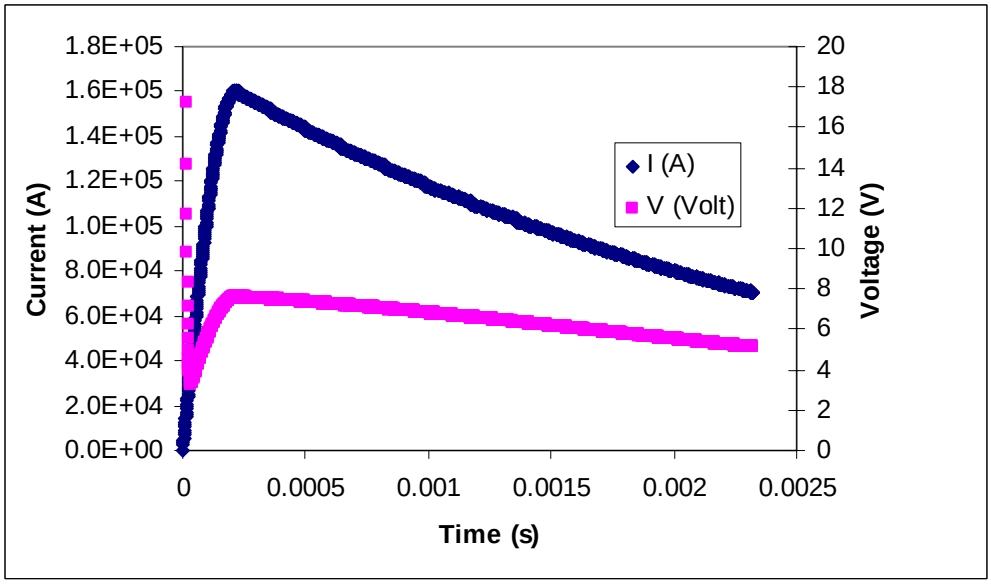

Figure 33. SPT-411A voltage drop versus time. (From Ref. 15.)

3. Switch Summary

The primary advantages of the SPT-411A over the ST-300A switch are lower voltage drop, smaller triggering requirement, longer life, and less expensive. Each SPT-411A and its associated trigger are expected to cost $2,400 and will require 16 switches (four per bank) resulting in a total cost of $38,400. The predicted switch life is also significantly greater than the ST-300A and is a factor of 10 greater than the predicted life of the capacitors. The ST-300A would require electrode replacement approximately every

6400 shots further adding to the cost of the switch, while the SPT-411A should last the life of the power supply without requiring maintenance. The disadvantage of the SPT-411A is that it provides a smaller growth margin than the ST-300A and would require two additional switches per bank to exceed 200 kA peak current per bank. Due to its long life expectancy, low maintenance requirements and cost, the SPT-411A will be used in this design.

C. DIODES

As discussed in section III.A, the GA capacitors selected for this design have a reverse voltage limit of 10% of the rated voltage or 1,100 V. In order to limit the reverse voltage on the capacitors, each bank must be protected by "crowbar" diodes. A diode string will be placed in parallel with the capacitor bank to prevent voltage reversal. As the voltage on the bank attempts to reverse the parallel diodes will be forward biased, as shown in Fig. 34. (The lines connect calculated data points and were produced by a PSpice model to illustrate this point.) The blue trace is the bank voltage, the green trace is the capacitor current, and the red trace is the diode current. It is important to note that the diode immediately begins to conduct at the peak bank current, and therefore must be rated to the same standard as the bank switches.

The SDD-303KT manufactured by SPCO will be used as the crowbar diodes. They have a peak reverse voltage of 6 kV and a peak non-repetitive half cycle current of 60 kA [17]. Three parallel stacks, each containing two diodes, will be required per bank. This will result in a total of six diodes per bank or 24 for the system. This diode has a pre-production cost of $700 resulting in a system cost of $16,800.

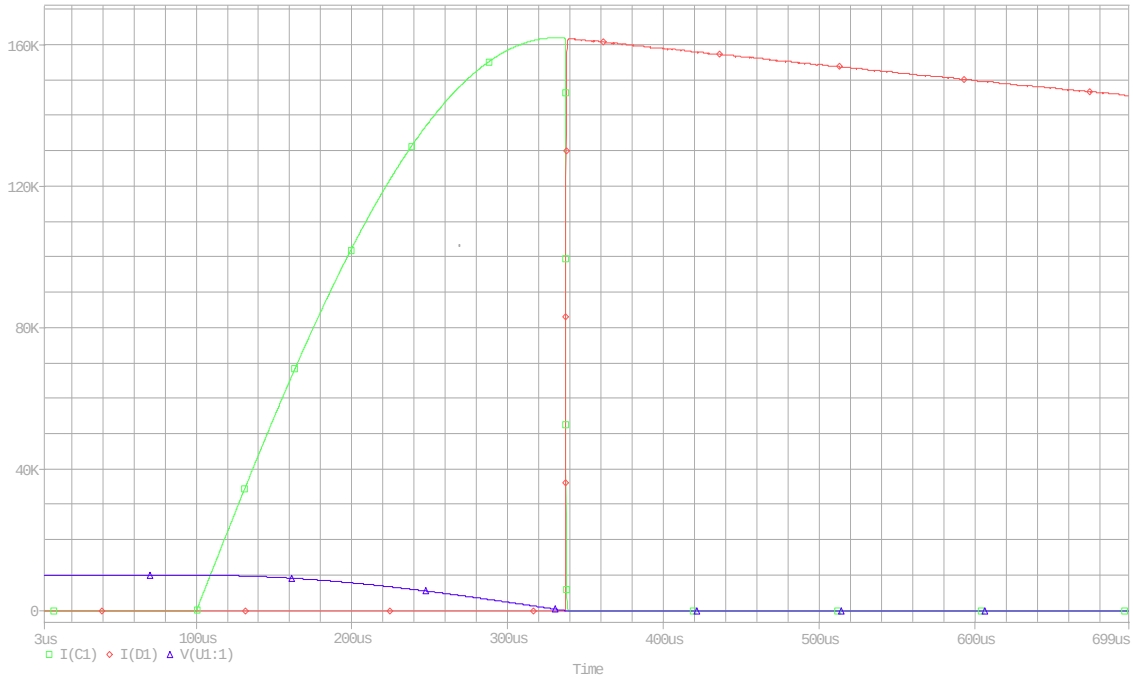

* Current in units of amps and voltage in units of volts.

Figure 34. Operation of crowbar diodes showing bank voltage (blue), capacitor current (green) and diode current (red).

D. CABLES

The cables for the system must be capable of handling large currents with minimal power loss. There are a limited number of cables capable of meeting the current carrying requirements for this design. One such example is made by Specialty Cable, part number 811-4981213, which is rated to greater than 300 kA. The cable resistance of 240 μΩ/m and an inductance of 120 nH/m was calculated from Ref. 18. It is anticipated that the power supply and the railgun will be located in the same room with less than five meters between them. A length of 10 m will result in a cable resistance of 2.4 mΩ and an inductance of 1.2 μH per bank. Cost of the cables is approximately $10 per foot for a total of $1,200, assuming two 5-m cables per bank and four banks.

E. CHARGING POWER SUPPLY

Aside from the capacitors and the switches, the charging power supply is the next most expensive parts of this design. The largest and only GA power supply that meets requirements is the CCS-12 series with a charge rate of 12 kJ/s [19]. The typical charge time for the GA, Series C, model 32327 capacitor is 60 s with a hold time of 30 s to

maximize the capacitors life [12]. At 12 kJ/s the entire system bank would reach full charge in 50 s. The CCS-12 power supply costs approximately $13,000.

F. MUZZLE SHUNTS

In order to allow the projectile to exit the barrel without causing damage to the ends of the rails, it is necessary to suppress the muzzle flash by providing an alternate path for the rail current. This current can be quenched by one of the following types of muzzle shunts: inductive, shorting switch, or resistive.

1. Inductive Muzzle Shunt

Inductive muzzle shunts have the desired characteristic of appearing to have infinite impedance at the beginning of the current pulse forcing all the current through the projectile. Over time the impedance of the inductor decreases slightly, allowing more current to flow through it. Once the projectile exits the barrel, the barrel current will attempt to flow through the muzzle inductor. The muzzle inductor again provides a large impedance due to the rapid change in current flow through it from the barrel current. Because current through an inductor cannot instantly change, a positive voltage spike occurs as the inductor attempts to oppose the change in current flow. Once current flow through the inductor equals the barrel current, the inductor voltage will adjust to attempt to maintain current in the circuit. In Fig. 35 the projectile exited the barrel at 2.8 ms with a 0.1 μH inductor used as a muzzle shunt to illustrate this effect. The green trace is the barrel current, the blue trace is the inductive muzzle shunt voltage, and red trace is the inductor current. For this case a 350 kA exit current produced a voltage spike of greater than 600 kV. Decreasing the size of the inductive shunt can minimize the voltage spike, but doing so will allow higher current flow through the inductor prior to the projectile exiting the barrel reducing system performance.

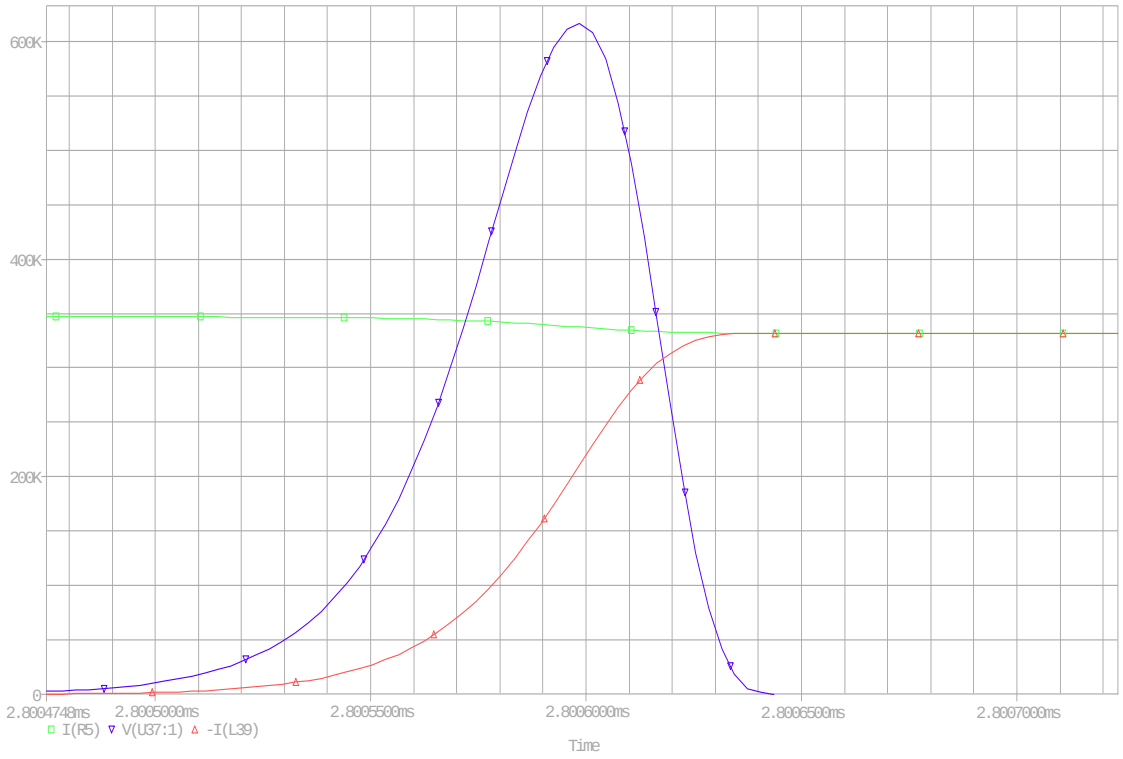

Figure 35. Inductive muzzle shunt voltage (blue; in V), inductor current (red; in A) and barrel current (green; in A).

2. Shorting Switch Shunt

Shorting switches offer the best opportunity to maintain full current through the projectile by short-circuiting the barrel just prior to the projectile exiting. The primary disadvantage to this technique is that the position of the projectile must be known fairly accurately in order to close the switch at the proper time, and it would require additional switches for the system. It is possible to sense the location of the projectile and trigger the shorting switch using a break wire circuit connected across the rails, similar to the circuit shown in Fig. 36 [20]. This technique will add to the complexity and expense of the overall system. The shorting switches must be sized to accommodate the maximum current expected when the projectile exits the barrel. From the previous discussion of railgun models summarized in Table 10, the requirement would be about 400 kA for a 10-kV shot. This could be done with one ST-300A switch costing about $12,200 for the switch and trigger or three SPT-411A's costing about $7,200.

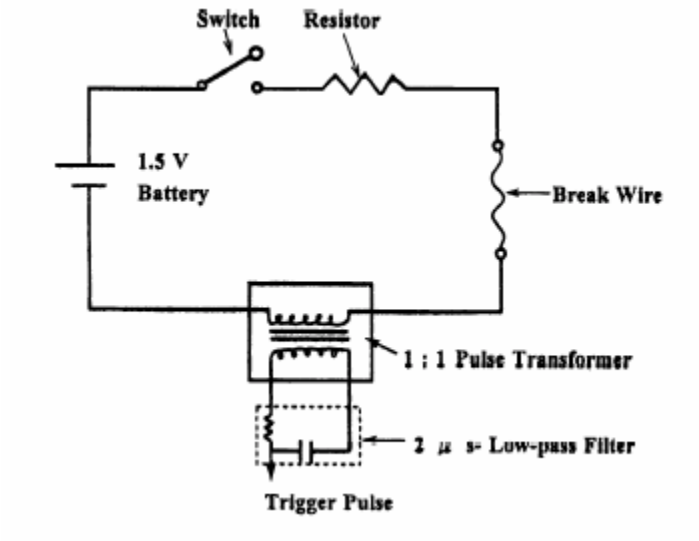

Figure 36. Break wire circuit. (From Ref. 20.)

3. Resistive Muzzle Shunt

Resistive muzzle shunts are the simplest of the three types of shunts considered for this design. They work in the same manner as the inductor with the exception that they maintain constant impedance over time. Typical values for a resistive shunt are between 1 mΩ to 5 mΩ. Since the projectile resistance is in the micro-ohm range the shunt will have little effect on the current seen by the projectile. It is also important to note that the shunt resistance must be significantly larger than the projectile resistance and its associated contact resistance as it moves down the barrel. While the projectile resistance is on the order of micro-ohm, an accurate value of the contact resistance has not yet been determined. The disadvantage to resistive shunts is that a portion of the energy left in the barrel gets converted to heat in the resistor. If this were a high repetition rate railgun system, the heating may become a factor. Since it is not anticipated that the gun will be fired more than a few time a day and will have sufficient cooling time between shots, the heating will not be a factor. In order to keep the design as simple and inexpensive as possible a resistive shunt of approximately 2 mΩ's will be used.

The only major component of the power supply not yet discussed is the pulse shaping inductors. The inductors can be designed and constructed as air-core type inductors, and the inductance can be adjusted by varying the number of turns. These should be relatively cheap and simple to construct locally.

Now that the primary components for the power supply have been identified, their characteristics can be more accurately modeled in a PSpice simulation. The PSpice model will provide a more rigorous electrical analysis of the power supply's performance and verify the MATLAB model developed in Chapter II. The next chapter will look at the PSpice results and attempt to relate those back to the performance model in Chapter II in order to provide a more accurate prediction of the total system performance.

THIS PAGE INTENTIONALLY LEFT BLANK

IV. FINAL DESIGN VERIFICATION

The MATLAB railgun model developed in Chapter II was useful for evaluating different power supply configurations and provided a rough estimate of the combined performance of the gun and power supply. However, the MATLAB model was not electrically robust enough to accurately predict the power supply's performance. A PSpice model using the component characteristics in Chapter III was developed to accomplish this task. This additional model will be used to refine the MATLAB results for the current pulse and then relate them to the gun's overall performance

A. PSPICE MODEL

In the previous chapter the major components necessary to construct the power supply and their characteristics were identified. The capacitor datasheet did not list an Equivalent Series Resistance (ESR), but did give an internal inductance rating of < 40 nH [12]. The switch data provided by SPCO showed a worst-case resistance of 72 μΩ, which will be the assumed value for this model. The resistance of the diodes at 50 kA peak current and 150°C is 160 μΩ [13]. Finally, the cable resistance and inductance are assumed to be 240 μΩ/m and 120 nH/m, respectively. Assuming that each bank has five meters of cable from the positive terminal of the power supply to the gun and another five meters from the gun back to the negative terminal, the total resistance and inductance will be 2.4 mΩ/bank and 1.2 μH/bank, respectively. Table 13 is a summary of these assumptions.

Component	Characteristics
Capacitors	L < 40 nH
Switches	R = 72 μΩ
Diodes	R = 160 μΩ
Cables	L =120 nH/m (1.2 μH/bank) R = 240 μΩ/m (2.4 mΩ/bank)

Table 13. Assumptions used in the PSpice model.

The capacitor inductances are not included in the model because they are insignificant when compared to the value of the pulse shaping inductor. Assuming the worst-case inductance of 40 nH and three capacitors in parallel per bank, the bank inductance would be 13.3 nH. This is negligible compare to the 7.7 μH of pulse shaping inductance. The switches were modeled by using a switch in series with a diode. A diode model from the PSpice library was chosen and the values of for the reverse hold-off voltage, B_v, and on-state resistance, R_s, were entered as 10 kV and 72μΩ, respectively. This is equivalent to two strings of SPT-411A thyristors connected in parallel with each string containing two devices connected in series. The crowbar diodes were modeled in the same manner as the diodes for the switches with B_v being set to 12 kV and R_s set to 106 μΩ. This is equivalent to three strings of SD-303KT diodes connected in parallel with each string containing two devices connected in series. The cable inductance of 1.2 μH was added to the pulse shaping inductors of each bank for a total of 8.9 μH, and the cable resistance of 2.4 mΩ was placed in series with the pulse shaping inductors of each bank. An additional resistor, *R5*, with a value 1 μΩ was added to provide a data collection point for the barrel current without causing a significant influence in the circuit. Figure 37 is the PSpice circuit schematic.

B. PREDICTED PERFORMANCE

The results of the PSpice model indicated that the current output of the power supply would be 527 kA, or 40 kA less than the MATLAB model predicted. The muzzle current was predicted to be 308 kA, or 13 kA less than the MATLAB model. Figure 38 is the PSpice model simulation graph. One factor contributing the reduction in peak current is the additional inductance from the cables, which was not accounted for in the MATLAB model. The cable resistance was also not included in the MATLAB model. The total series resistance seen by a bank is 2.4 mΩ plus the switch and diode resistance of 72 μΩ and 106 μΩ, respectively. Another effect not modeled in the MATLAB code is the paralleling of the banks after each one is fired. Once all banks have fired and each set of crowbar diodes are conducting, the total impedance of the power supply is reduced by a factor of four. This implies that the system inductance will be one-fourth of its original value and allow the current to fall of faster than what would be indicated by the MATLAB model.

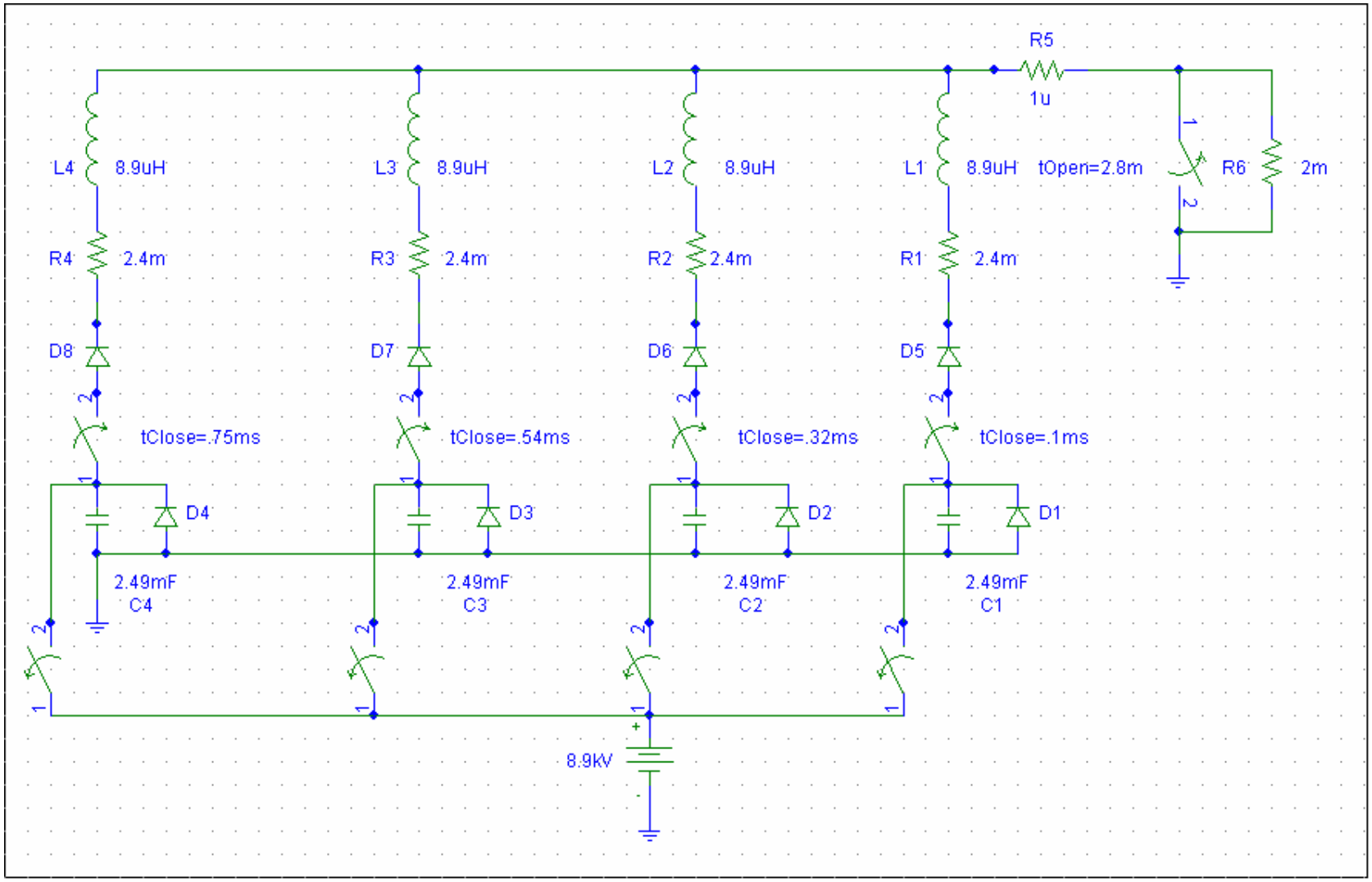

Figure 37. PSpice power supply circuit schematic (All resistances in ohms)

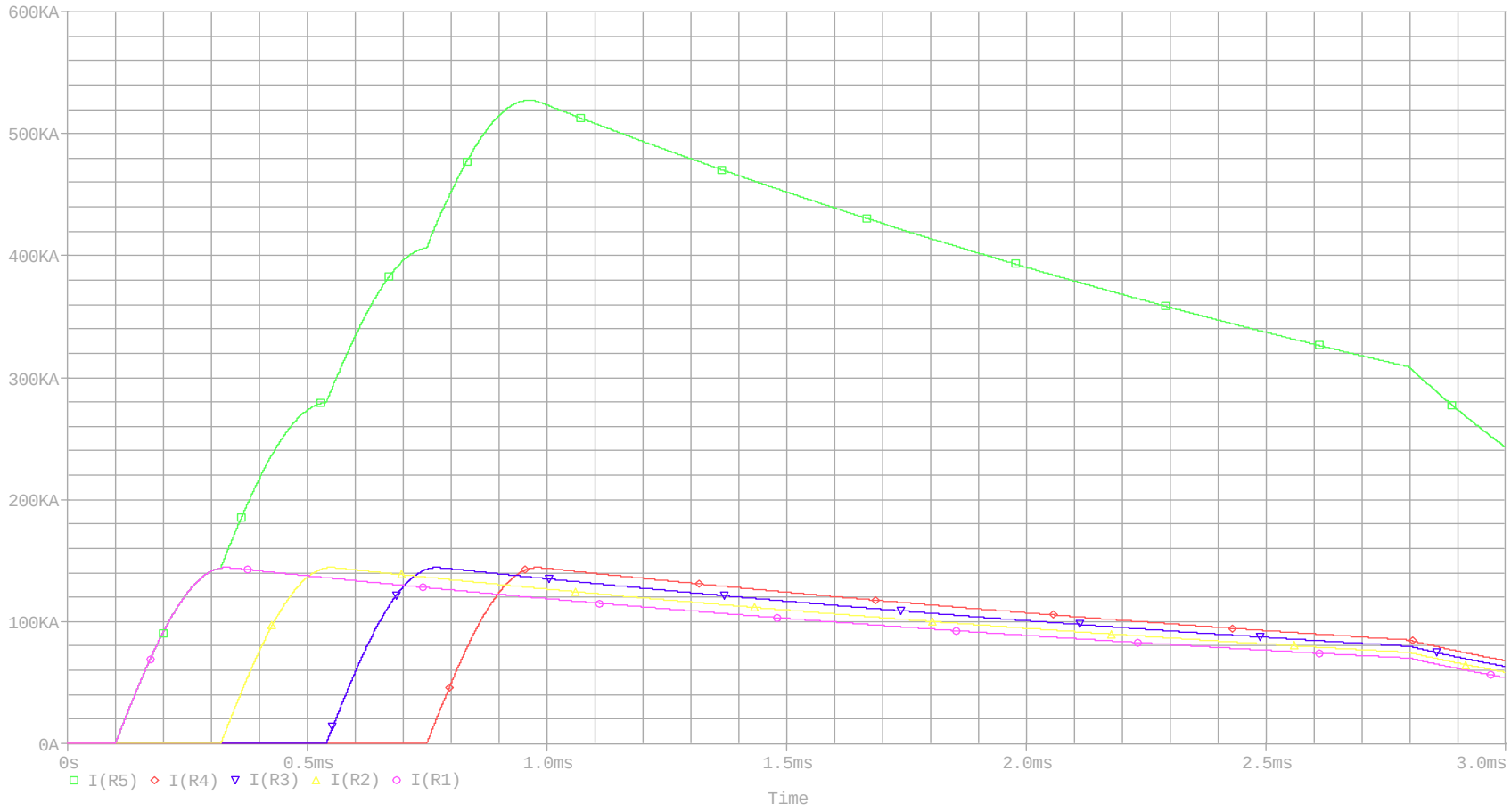

Figure 38. PSpice simulation graph (Y-axis is current in units of amps).

Since the PSpice model does not incorporate any of the projectile performance equations, it is necessary to go back to the MATLAB model to determine the effect that these differences will have on the gun's performance. The values for *C, L* and *R* will be varied in the MATLAB model to produce the desired waveform. Figure 39 is the MATLAB railgun performance model graphs for the PSpice predicted waveform and Table 14 contains the summary of the railgun performance model outputs.

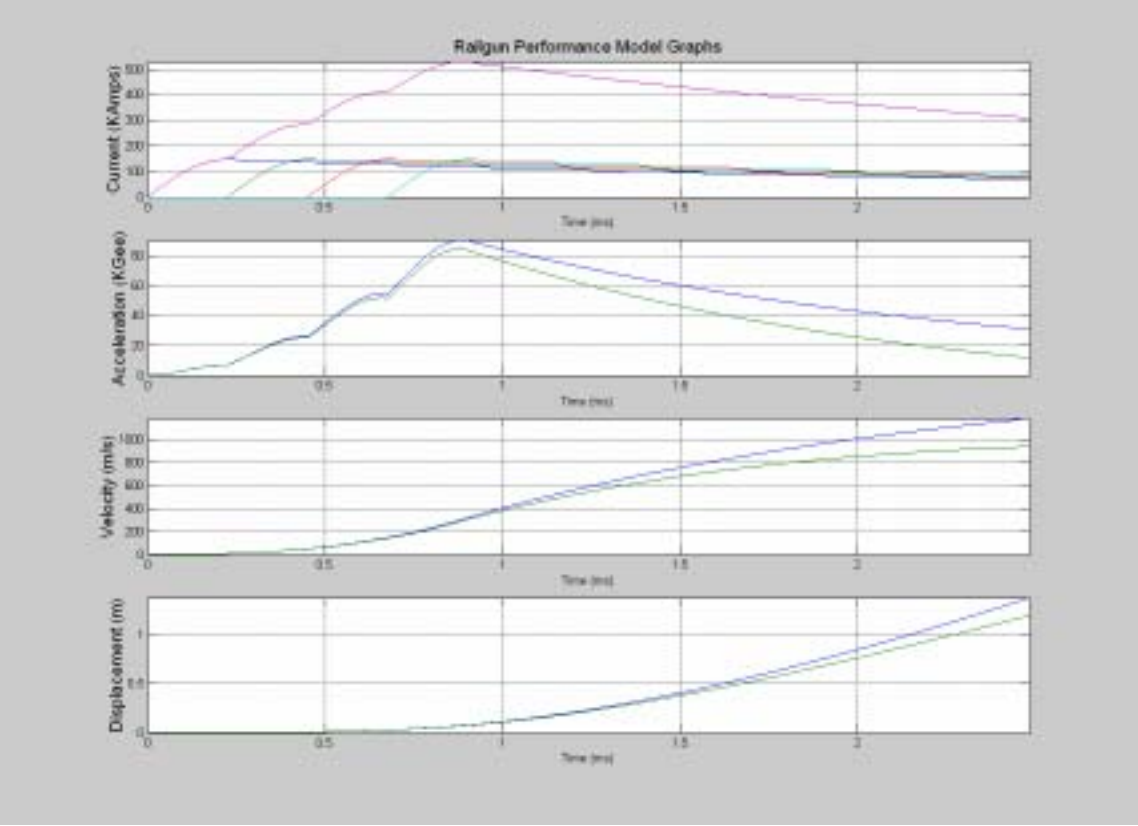

Figure 39. MATLAB performance model graphs for the PSpice current pulse.

The decrease in predicted performance based on the PSpice current pulse was not significant. The muzzle velocity was estimated to be 932 m/s and the effective-barrel-length decreased to 0.90 m. In an attempt to fully meet the design requirements the firing voltage was increased from 8.9 kV to 10 kV in the PSpice model without modifying other system parameter. The output current pulse maintained its previous form and had a

Muzzle Velocity	936 m/s
Current Density	33.0 kA/cm^2
Peak Current	528 kA
Exit Current	309kA
Effective-barrel-length	0.90 m

Table 14. Summary of the railgun performance model outputs.

predicted peak current of 592 kA with an exit current of 374 kA. As in the previous case, the PSpice current pulse was evaluated using the MATLAB model. Those results are shown in Fig. 40 and Table 15. Increasing the bank firing voltage to 10 kV resulted in a predicted muzzle velocity of 1071 m/s and an effective-barrel-length of 1.08 m with a current density of 36.0 kA/cm^2. Lowering the bank voltage to a value between 8.9 kV and 10 kV could reduce the muzzle current, but this will not result in a significant improvement. The power supply schematic in Fig. 38 produces a model that meets the design goals and will be the final design configuration.

Once the cable inductance was included in the MATLAB model, the current peaks for the two models were within 1%. If the cable resistance assumption is included, the current pulse fall-off-rate for the MATLAB model exceeds the PSpice fall-off-rate, which resulted in an muzzle exit current of 275 kA.

Muzzle Velocity	1071 m/s
Current Density	36.0 kA/cm^2
Peak Current	592 kA
Exit Current	347 kA
Effective-barrel-length	1.08 m

Table 15. Final railgun and power supply performance summary.

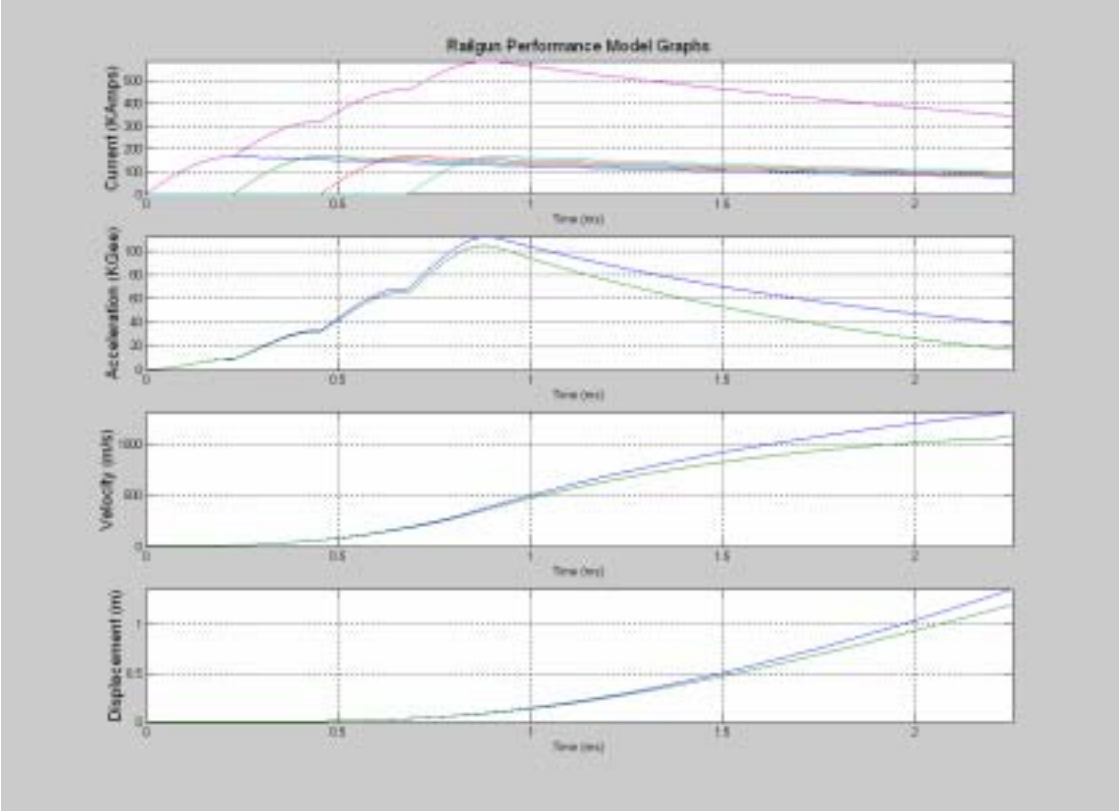

Figure 40. Final railgun and power supply performance graphs.

C. PARTS LIST AND COST

Table 16 summarizes the necessary components to build this power supply based on the circuit diagram in Fig. 38, but does not include the inductors, control and timing circuits for the switches, or any data collection and monitoring equipment. Also not included in the total cost are the materials for the construction of the protective housing for the high power components and the cost of lab support personnel to operate and maintain the system. These additional costs could result in the ultimate price of the power supply exceeding of $200,000.

Component	Manufacturer	Part number	Quantity	Total Cost
Capacitors	General Atomic	32327	12	$60,000
Switches	Silicon Power	SPT-411A	16	$38,400
Diodes	Silicon Power	SDD-303KT	24	$16,800
Charging Power Supply	General Atomics	CCS-12	1	$13,000
Cables	Specialty Cable	811-4981213	120 ft	$1,200
			Material Cost	**$129,400**

Table 16. Power supply primary parts list parts list.

There is a potential to reduce the total cost of the power supply by having masters level students from the Physics and Electrical Engineering departments design and construct the timing and control circuits, and the capacitor charging power supply. Additionally, if the velocity requirements were reduced to 800 m/s, four capacitors (one from each bank) and eight switches (two from each bank) could be remove from the design for a total savings of $39,200. The reduction of the peak current per bank from 160 kA to less than the 147 kA switch limit would allow the removal of two switches per bank. The engineers at SPCO should verify the performance of the SPT-411A under the new operating conditions.

D. CONCLUSION AND RECOMMENDATIONS

This thesis has demonstrated that it is theoretically possible to design a 1.2-m railgun and power supply that will accelerate a 172-g projectile to a velocity of 1000 m/s. Using Equations 1.10 and 1.14, a MATLAB model was constructed to evaluate the effectiveness of both the single and multiple-bank configurations. By systematically varying the model's inductance and capacitance, system design spaces for velocity, current density, muzzle current and effective-barrel-length were identified. These design spaces were then used in conducting trade-off studies to optimize the system performance. Because of the cost associated with construction of such a large power supply, a PSpice

model was developed to verify the MATLAB model in a more electrically rigorous environment. The two models agreed to within 4 kA on the predicted peak current. This agreement helped to validate the utility of the MATLAB model as an effective conceptual design tool. Finally this design shows that by sequentially firing smaller multiple capacitor banks, the overall system capacitance required to achieve a velocity of 1000 m/s can be reduced from 21.58 mF to 9.96 mF. This results in a cost reduction of $70,000 for the capacitors alone. It is recommended that the required parts to assemble one bank are purchased and further testing is done to verify the model and assumptions made in this thesis.

THIS PAGE INTENTIONALLY LEFT BLANK

APPENDIX A. MATLAB SINGLE OR MULTI-BANK RAILGUN PERFORMANCE MODEL

The following MATLAB code generated the figures and values used in the trade-off studies between the single-bank and multiple-bank scenarios of Chapter II. The code was used again in Chapter IV to relate the results of the PSpice power supply model to the performance of the railgun. A detailed discussion of the equation used in this model can be found in Section II.B.

```
% LT Dwight Warnock
% RAILGUN POWER SUPPLY THESIS
% September, 2003

clear

%%%%%%%%%%%%%%%%%%%%%%%%%%%%%%%%%%%%%%%%%%%%%%%%%%%%%%%%%%%%%%%%
%                              Input variables
%%%%%%%%%%%%%%%%%%%%%%%%%%%%%%%%%%%%%%%%%%%%%%%%%%%%%%%%%%%%%%%%


promptG  = {'Barrel length in meters','Rail Spacing in cm','RailHeight in cm',
   'Augmentation rail spacing in mm','Rail width in mm'};
titleG   = 'Enter Railgun Characteristics';
linesG= 1;
defG     = {'1.2','1.6','1.6','1.3','6.25'};
G_input  = inputdlg(promptG,titleG,linesG,defG);
x=str2num(G_input{1});                  %Barrel Length
y=str2num(G_input{2})*1e-2;             %Bore width
h=str2num(G_input{3})*1e-2;             %Bore height
s=str2num(G_input{4})*1e-3;             %Augmentation rail spacing
w=str2num(G_input{5})*1e-3;             %Rail width

promptP  = {'Projectile length in cm','Projectile Material Density in g/cm^3',
   'Initial Velocity in m/s','Rail Coating viscosity in cP',
   'Rail Coating Layer Thickness in microns'};
titleP   = 'Enter Projectile Characteristics';
linesP= 1;
defP     = {'15','13.4','0','65','6'};
P_input  = inputdlg(promptP,titleP,linesP,defP);
l=str2num(P_input{1})*1e-2;             %Projectile length
rho=str2num(P_input{2})*1e3;            %Projectile density
velocity_int=str2num(P_input{3});       %Initial velocity
vis=str2num(P_input{4});                %Rail coating viscosity
```

```
thickness=str2num(P_input{5})*1e-6;        %Layer thickness of rail coating material


m=rho*h*y*l;                               %Projectile mass in Kg
uo=4*pi*1e-7;                              %Permeability of Air.
velocity_friction=[0];                     %Intitializes velocity with friction equation


promptC  = {'Enter PFN Voltage in Volts:','System resistance in Ohms',
   'Enter individual capacitor size in mF','Number of Caps. in Bank #1',
   'Number of Caps. in Bank #2','Number of Caps. in Bank #3',
   'Number of Caps. in Bank #4'};
titleC   = 'Enter PFN characteristics';
linesC= 1;
defC     = {'10000','.003','.830','1','1','1','1'};
C_input  = inputdlg(promptC,titleC,linesC,defC);
V=str2num(C_input{1});                     %Capacitor voltage
R=str2num(C_input{2});                     %Charateristic system resistance in ohms
C=str2num(C_input{3})*1e-3;                %Individual Capacitor Value
C1=str2num(C_input{4})*C;                  %Capacitance of segement one in farads
C2=str2num(C_input{5})*C;                  %Capacitance of segement two in farads
C3=str2num(C_input{6})*C;                  %Capacitance of segement three in farads
C4=str2num(C_input{7})*C;                  %Capacitance of segement four in farads


promptL  = {'Enter System Inductance','L1:','L2','L3','L4'};
titleL   = 'Input for System inductances in microHeneries';
linesL= 1;
defL     = {'2.5','0','0','0','0'};
L_input  = inputdlg(promptL,titleL,linesL,defL);
L=str2num(L_input{1})*1e-6;                %Charateristic system inductance in heneries
L1=str2num(L_input{2})*1e-6;               %Inductance of bank one in heneries
L2=str2num(L_input{3})*1e-6;               %Inductance of bank two in heneries
L3=str2num(L_input{4})*1e-6;               %Inductance of bank three in heneries
L4=str2num(L_input{5})*1e-6;               %Inductance of bank four in heneries

promptT  = {'Enter Bank #2 Delay in mSec:','Enter Bank #3 Delay in mSec:'
   ,'Enter Bank #4 Delay in mSec:'};
titleT   = 'Capacitor Bank Time Delays from the Peak of the previous bank';
linesT= 1;
defT     = {'0','0','0'};
T_input  = inputdlg(promptT,titleT,linesT,defT);
t_delay_2=str2num(T_input{1})*1e-3;      %Time delay from the I_peak_1 to fire bank 2
t_delay_3=str2num(T_input{2})*1e-3;      %Time delay from the I_peak_2 to fire bank 3
t_delay_4=str2num(T_input{3})*1e-3;      %Time delay from the I_peak_3 to fire bank 4
```

```
%%%%%%%%%%%%%%%%%%%%%%%%%%%%%%%%%%%%%%%%%%%%%%%%%%%%%%%%
%                                    Calculating L_prime
%%%%%%%%%%%%%%%%%%%%%%%%%%%%%%%%%%%%%%%%%%%%%%%%%%%%%%%%

        % Unaugmented case
L_prime_u=(uo/(2*pi))*log((w+y)^2/w^2);

        % Augmented case
temp=[];
temp1=0;
for i=0:10000
   yi=(w/2)+y*i/10001;
   temp=(1/yi+1/(w+s+yi))*2*y/10000;
   temp1=temp1+temp;
end
L_prime_a=uo/(2*pi)*temp1;
L_prime=L_prime_a;

%%%%%%%%%%%%%%%%%%%%%%%%%%%%%%%%%%%%%%%%%%%%%%%%%%%%%%%%
%                                              Current profiles
%%%%%%%%%%%%%%%%%%%%%%%%%%%%%%%%%%%%%%%%%%%%%%%%%%%%%%%%

        % Peak Current due to capacitance
I_peak_1=V*sqrt(C1/(L1+L));
I_peak_2=V*sqrt(C2/(L2+L));
I_peak_3=V*sqrt(C3/(L3+L));
I_peak_4=V*sqrt(C4/(L4+L));

        % Time to Peak Current
t_peak_1=pi*sqrt((L1+L)*C1)/2;
t_peak_2=t_peak_1+t_delay_2+pi*sqrt((L2+L)*C2)/2;
t_peak_3=t_peak_2+t_delay_3+pi*sqrt((L3+L)*C3)/2;
t_peak_4=t_peak_3+t_delay_4+pi*sqrt((L4+L)*C4)/2;

        % omega per segment
w_1=1 / sqrt((L+L1)*C1);
w_2=1 / sqrt((L+L2)*C2);
w_3=1 / sqrt((L+L3)*C3);
w_4=1 / sqrt((L+L4)*C4);

        % Current Pulses
dt=1e-6;
for j=2:10000
   t(j)=j*dt;
```

```
        % Current Pulse 1
    if t(j) <= t_peak_1;
       I1(j)=I_peak_1*sin(w_1*t(j));
    else
       I1(j)=I_peak_1*exp(-R*(t(j)-t_peak_1)/(L+L1));
    end

        % Current Pulse 2
    if t(j) < (t_peak_1+t_delay_2);
       I2(j)=0;
    elseif t(j) <= t_peak_2
       I2(j)=I_peak_2*sin(w_2*(t(j)-(t_peak_1+t_delay_2)));
    else
       I2(j)=I_peak_2*exp(-R*(t(j)-t_peak_2)/(L+L2));
    end

        % Current Pulse 3
    if t(j) < (t_peak_2+t_delay_3);
       I3(j)=0;
    elseif t(j) <= t_peak_3
       I3(j)=I_peak_3*sin(w_3*(t(j)-(t_peak_2+t_delay_3)));
    else
       I3(j)=I_peak_3*exp(-R*(t(j)-t_peak_3)/(L+L3));
    end

        % Current Pulse 4
    if t(j) < (t_peak_3+t_delay_4);
       I4(j)=0;
    elseif t(j) <= t_peak_4
       I4(j)=I_peak_4*sin(w_4*(t(j)-(t_peak_3+t_delay_4)));
    else
       I4(j)=I_peak_4*exp(-R*(t(j)-t_peak_4)/(L+L4));
    end


        % Total Current Pulse
I_total(j)=I1(j)+I2(j)+I3(j)+I4(j);

        % Acceleration
accel(j)=L_prime*I_total(j)^2/(2*m);


        % Velocity
v_temp(j)=accel(j)*dt;
velocity(j)=velocity_int+sum(v_temp);
```

```
	%Displacement
d_temp(j)=velocity(j)*dt;
displacement(j)=sum(d_temp);

	%Friction Effects
friction(j)=2*l*h*velocity_friction(j-1)*(vis/1000)/(thickness*m);
accel_friction(j)=L_prime*I_total(j)^2/(2*m)-friction(j);

v_tempfric(j)=accel_friction(j)*dt;
velocity_friction(j)=velocity_int+sum(v_tempfric);

d_tempfric(j)=velocity_friction(j)*dt;
displacement_friction(j)=sum(d_tempfric);

   if displacement_friction(j) > x
      break
   end
   if velocity_friction(j) < 0
      break
   end
end

%%%%%%%%%%%%%%%%%%%%%%%%%%%%%%%%%%%%%%%%%%%%%%%%%%%
%                                   Model Output Data
%%%%%%%%%%%%%%%%%%%%%%%%%%%%%%%%%%%%%%%%%%%%%%%%%%%

	%Minimum current to maintain acceleration
I_min=sqrt(max(friction)*2*m/L_prime)/1000;
min_I=num2str(I_min);

	%Mass
m1=m*1000;
mass=num2str(m1);
A=l*h;

	%Maximum Output Current
Jmax=num2str(max(I_total)/(1e7*A));

	%Muzzle Velocity
Vmuz=num2str(max(velocity_friction(j)));

	%Effective Barrel Length
[z,ac]=find(accel_friction>2.02e5);
[C,k]=max(ac);
barrel_effective=displacement_friction(C);
```

```
%%%%%%%%%%%%%%%%%%%%%%%%%%%%%%%%%%%%%%%%%%%%%%%
%                                    Plots
%%%%%%%%%%%%%%%%%%%%%%%%%%%%%%%%%%%%%%%%%%%%%%%

figure(1)

subplot(4,1,1)
plot((t*1000),(I1/1e3),(t*1000),(I2/1e3),(t*1000),(I3/1e3),(t*1000),(I4/1e3),(t*1000),(I_t
otal/1e3))
title('Railgun Performance Model Graphs')
ylabel('Current (KAmps)');
xlabel(['Max Current ',num2str(max(I_total)/1e3), ' (KAmps),   Max Current Density
(KAmps/cm^2) = '
   ,Jmax, ', Current at muzzle exit ',num2str(I_total(j)/1e3),' (KAmps)']);
grid
axis tight
subplot(4,1,2)
plot((t*1000),(accel/9800),t*1000,(accel_friction/9800))
xlabel(['Acceleration at muzzle exit ',num2str(accel_friction(j)/9800),' (KGee)   Projectile
Mass = '
   ,mass,' (g) length = 'num2str(l*100),' (cm)'])
ylabel('Acceleration (KGee)')
grid
axis tight
subplot(4,1,3)
plot((t*1000),velocity,t*1000,velocity_friction)
ylabel('Velocity (m/s)')
xlabel(['Muzzle velocity (m/s) = ',Vmuz,'        Effective barrel length
',num2str(barrel_effective),
   ' meters,    f = ',num2str(I_total(j)/max(I_total)),'    Minimum Current to maintain ve-
locity = '
   , min_I,'KAmps']);
grid
axis tight
subplot(4,1,4)
plot((t*1000),displacement,t*1000,displacement_friction)
axis tight
xlabel('Time (ms)')
ylabel('Displacement (m)')
grid
figure(2)
subplot(4,1,1)
plot(displacement_friction,(I1/1e3),displacement_friction,(I2/1e3),displacement_friction,
(I3/1e3),
displacement_friction,(I4/1e3),displacement_friction,(I_total/1e3))
title('Railgun Performance Model Graphs')
```

```
ylabel('Current (KAmps)');
xlabel(['Max Current ',num2str(max(I_total)/1e3), ' (KAmps), Max Current Density (KAmps/cm^2) = '
   ,Jmax, ', Current at muzzle exit ',num2str(I_total(j)/1e3),' (KAmps)']);
grid
axis tight
subplot(4,1,2)
plot(displacement_friction,(accel_friction/9800))
xlabel(['Acceleration at muzzle exit ',num2str(accel_friction(j)/9800),' (KGee) Projectile Mass = '
   ,mass,' (g) length = 'num2str(l*100),' (cm)'])
ylabel('Acceleration (KGee)')
grid
axis tight
subplot(4,1,3)
plot(displacement_friction,velocity_friction)
ylabel('Velocity (m/s)')
xlabel(['Muzzle velocity (m/s) = ',Vmuz,' Effective barrel length ',num2str(barrel_effective),
   ' meters, f = ',num2str(I_total(j)/max(I_total)),' Minimum Current to maintain velocity = '
   , min_I,'KAmps']);
grid
axis tight
subplot(4,1,4)
plot(displacement_friction,t*1000)
axis tight
xlabel('Displacement (m)')
ylabel('Time (msec)')
grid
```

THIS PAGE INTENTIONALLY LEFT BLANK

APPENDIX B. SINGLE-BANK DESIGN DETAILS

This appendix describes the trade-off off studies to produce the final results of the single-bank model discussed in Section II.B. It is similar to the multiple-bank design described in Section II.C.

The objectives were:

1. Minimize the capacitance require to meet the desired muzzle velocity.
2. Minimize the barrel current when the projectile exits.
3. Optimize the current pulse to maximize the barrel usage.
4. Maintain the projectile current density as low as possible.

The above objectives are in conflict with each other for the following reasons. In order to optimize the barrel usage it is necessary to produce a flatter pulse than the one shown in Fig. 15. The parameters that control the pulse shape are L, C and R. Since the resistance term is an intrinsic value of the system, it cannot be easily decreased, and it is undesirable to increase it. For this reason resistance will be treated as a constant. An increase in inductance will cause the desired effect of reducing the peak current and slowing the inductive phase rate of decrease. This will have the positive effect of reducing the current density and lengthening the pulse to closer match the barrel length, but will results in a higher barrel current when the projectile exits. Because acceleration is proportional to the current squared, the average acceleration is lower for the increased inductance case and subsequently causes the muzzle velocity to also be lower. In order to compensate for the loss in velocity, it is necessary to increase the amount of capacitance in the power supply, assuming a constant voltage. This requirement is in conflict with stated objective to minimize the capacitance and also results in an increased peak current and a current density that may be higher than in the lower inductance case.

From the above discussion it is clear that designing a power supply for a railgun is an exercise in system optimization. In order to identify the design space for the single-bank model, plots of muzzle velocity, muzzle current, current density, and effective-barrel-length versus inductance and capacitance were constructed. These plots were then

used to estimate the size of the capacitor bank and system inductance. The estimates were when put back into the single-bank performance model for further refinement and analysis.

Before continuing it is necessary to define effective-barrel-length. After the current pulse peaks it begins to fall off exponentially and acceleration decreases as square of the current. The acceleration will eventually decrease to the point that it will equal the frictional losses and the projectile will stop gaining speed. The point at which acceleration stops could be called the effective-barrel-length since the projectile does not gain velocity after this point. If the current is not maintained at the value corresponding to zero acceleration, as calculated in Equations 2.5 and 2.6, the projectile will lose velocity. Upon further examination of the plots of acceleration and velocity verses displacement, it is clear that significant acceleration ends well before the zero acceleration. Based on the plots in Fig. 41 and the zero acceleration definition, the effective-barrel-length would be approximately 1.2 m for this configuration when, in reality, significant acceleration ended just after 0.8 m. A better definition for effective-barrel-length is when the acceleration decreases to twice the frictional losses. Applying this definition gives an effective-barrel-length of 0.82 m. The importance of effective-barrel-length is that it can be used to help match the gun with the power supply. By using a greater portion of the gun rails to accelerate the projectile, the damage caused by the high currents and heat can be more effectively managed and the barrel life extended.

Now that effective-barrel-length and its importance to the design are better understoofd , it is time to look at the design trade-off graphs. The gun parameters and assumptions used to develop these graphs are as listed in Table 17.

The two most important aspects of the design are meeting the minimum muzzle velocity of 1000 m/s and the maximum projectile current density of 40 kA/cm^2. The acceptable combinations of capacitance and inductance that will meet the velocity requirement is any combination on or above the 1000 m/s contour line in Fig. 42. It is not surprising that the lowest capacitance capable of providing 1000 m/s corresponds to the minimum inductance value of $2.5\,\mu H$. It is also important to point out that in the interest

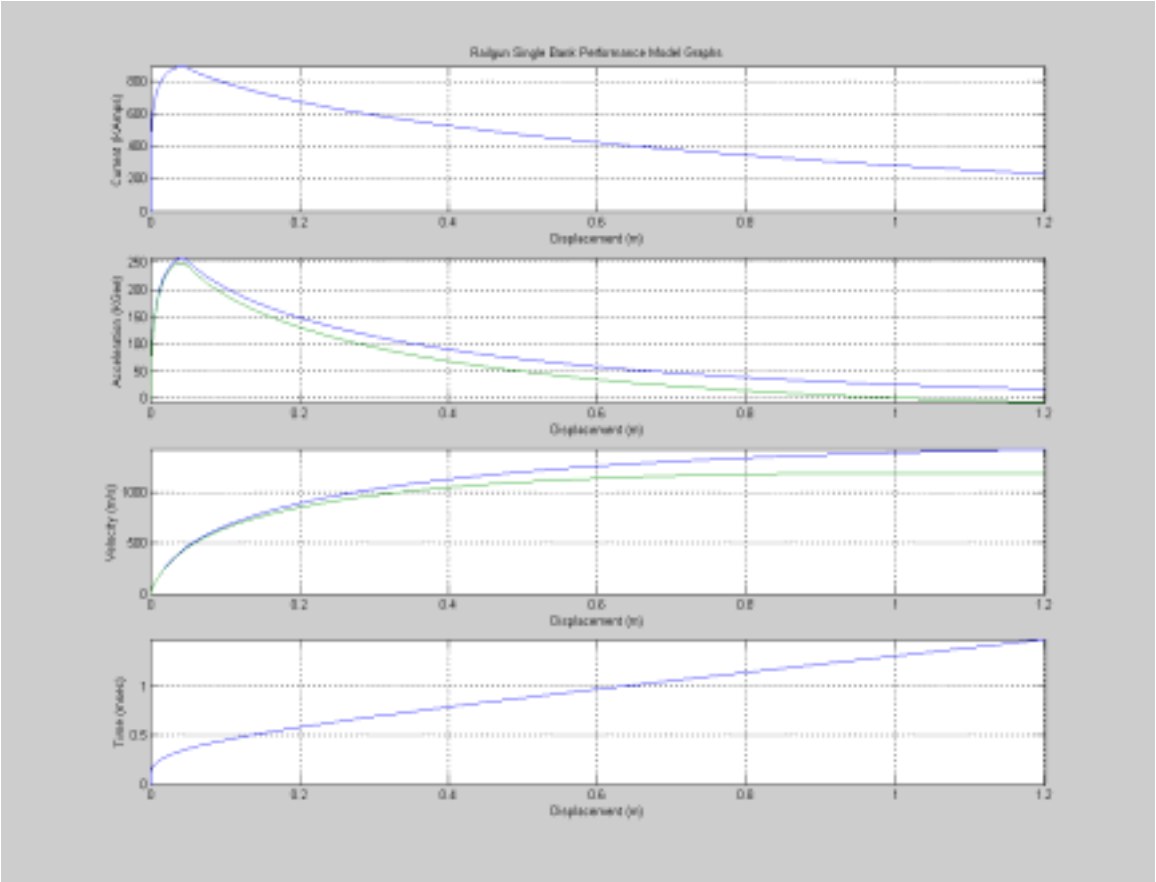

Figure 41. Single-bank railgun performance model versus displacement.

Barrel length: 1.2 m	Bore height: 1.6 cm	Bore width: 1.6 cm
Inductance minimum: 2.5 μ H	Resistance: 0.003 Ω	L' based on Eq. 1.13: 1.1 μH/m
Voltage: 10 kV	Projectile Density: 6.7 g/cm^3	Projectile weight: 171.5 g
Projectile Length: 10 cm	Silver paste viscosity: 65 cP	Maximum projectile current density: 40 kA/cm^2

Table 17. Design graph railgun model parameters.

of minimizing the capacitance and thus the system cost the final design point should be as close to the 1000 m/s contour as practical. Similarly, any combination of capacitance and inductance below the 40 kA/cm^2 contours in Fig. 43 will result in an acceptable current density. As expected, when the inductance goes up the current density decreases for a given capacitance since the peak current value is decreased. The overlapping area be-

tween the velocity design space and current density design space is considered the system design space. Any combination of capacitance and inductance that falls inside the red triangle areas in Fig. 42 and Fig. 43 will result in a design that meets the two previously stated design requirements.

The next step is to attempt to optimize the system to maximize the effective-barrel-length and minimize the muzzle current while staying inside the system design space. To do this it is necessary to explore the design space as it relates to the effective-barrel-length and muzzle current contour plots of Fig. 44 and Fig. 45, respectively. Again, there is a conflict between minimizing the capacitance while optimizing the effective-barrel-length and muzzle current. The lower left corner of the design space triangle represents the best possible solution for minimizing capacitance and muzzle current, but is the worst case for effective-barrel-length and current density. The upper right corner represents the best-case current density solution, but is also the worst-case capacitance solution and sub-optimal for barrel length and muzzle current. The upper left corner is the worst-case solution for capacitance, muzzle current, and current density, but it does provide the maximum use of the barrel. In this design the overriding concern is the cost of the system which is dominated by the cost of the capacitors. It is for this reason that solutions near the lower left corner will be preferred over solutions in the upper right corner.

The GA Series C, 830-μF, 11-kV capacitor was chosen as the reference capacitor for use in this design [12]. To meet the minimum acceptable capacitance to remain in the design space will require 26 capacitors resulting in a total bank capacitance of 21.58 mF and corresponds to inductance values in the very narrow range of 5.25 to 5.5 μH. The final solution for the single-bank model is discussed in Section II.B.

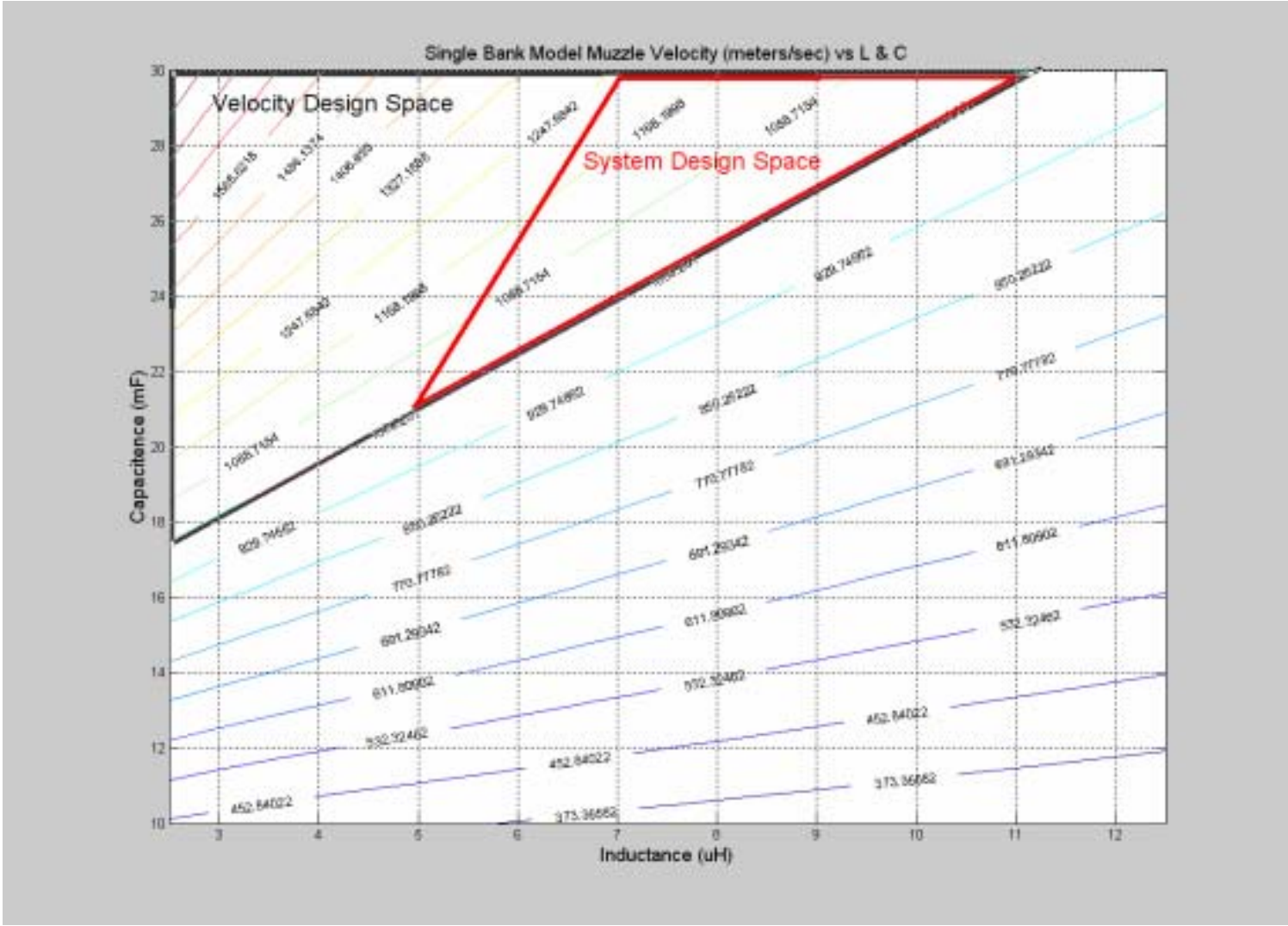

Figure 42. Single-bank muzzle velocity contour plot.

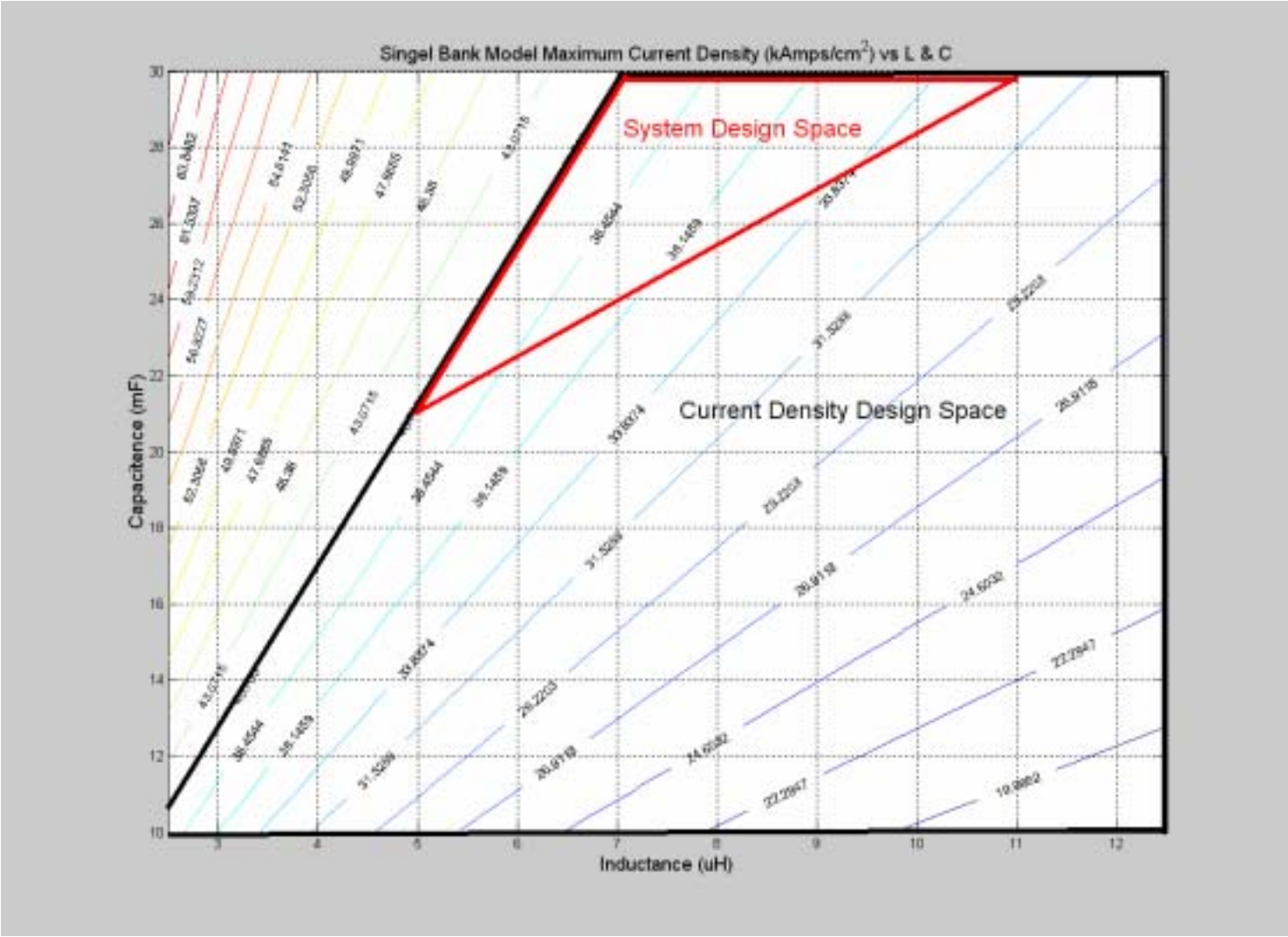

Figure 43. Single-bank current density contour plot.

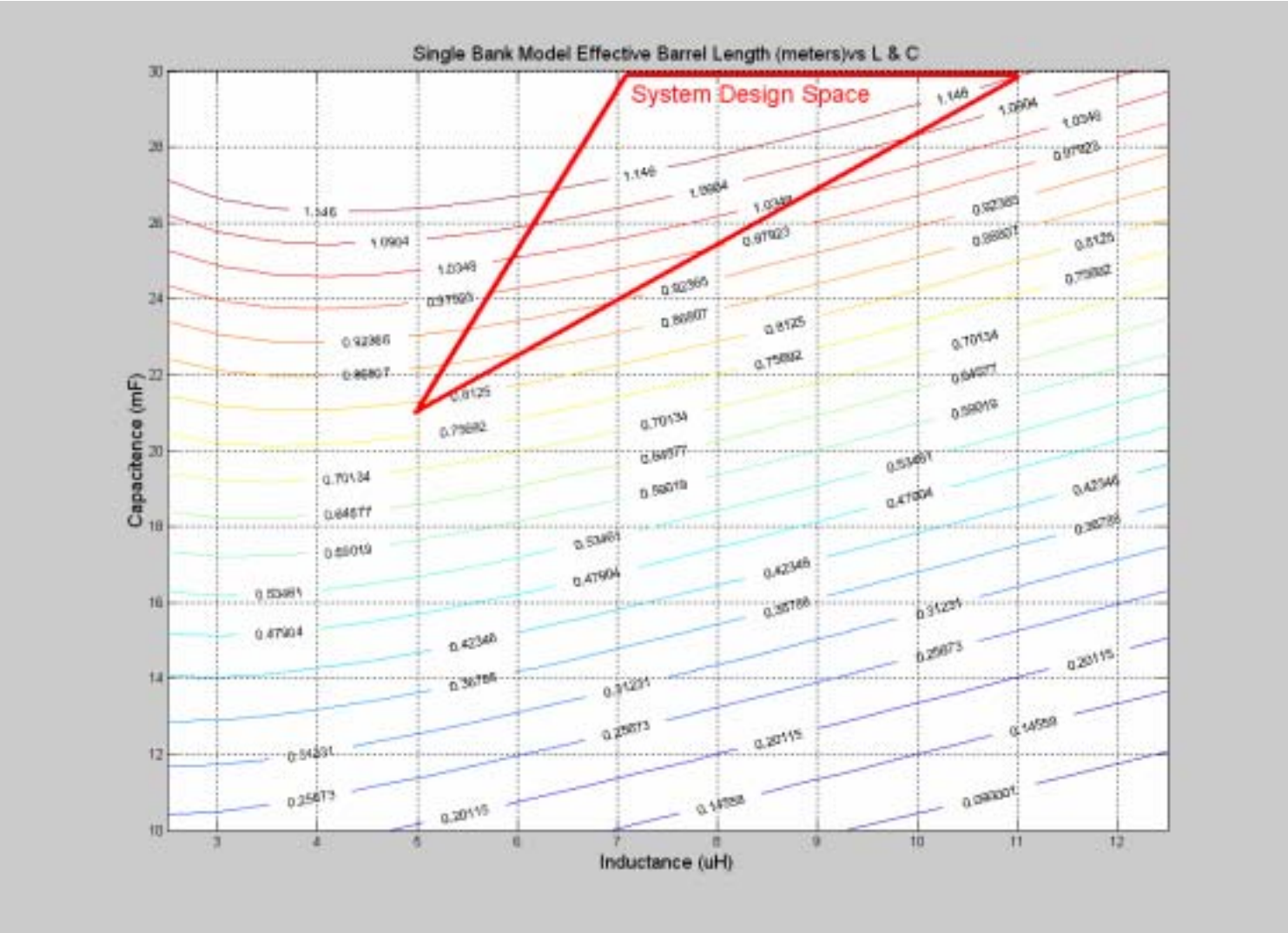

Figure 44. Single-bank effective-barrel-length contour plot.

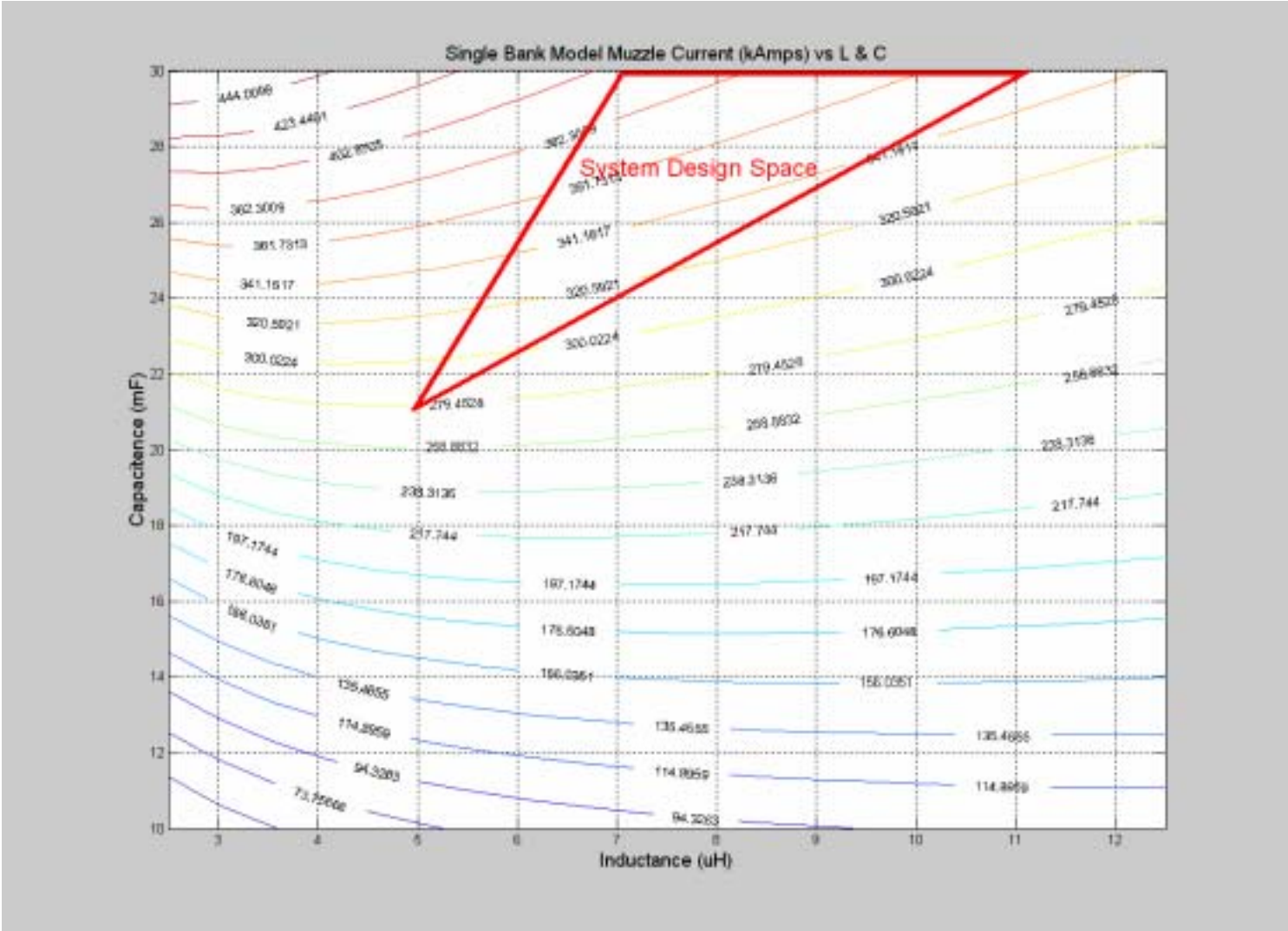

Figure 45. Single-bank muzzle current contour plot.

LIST OF REFERENCES

[1] Office of the Chief of Naval Operations, *Sea Power 21*, Washington, D.C.: Department of the Navy, October 2002.

[2] Office of the Chief of Naval Operations, Message, Date Time Group: 152120ZNOV02.

[3] Chester Petry, "Ship Integration Introduction," presented at the Electro-Magnetic Launch Workshop, Austin, Texas, November 2001.

[4] Chester Petry, "Hypersonic Naval Railgun," seminar at the Naval Postgraduate School, Monterey, California, April 2003.

[5] I.R. McNab, "Early Electric Gun Research," *IEEE Transactions on Magnetics*, Vol. 35, No. 1, pp. 250-261, 1999.

[6] Allen S. Feliciano, "The Design and Optimization of a Power Supply for a One-meter Electromagnetic Railgun," Master's thesis, Naval Postgraduate School, Monterey, California, December 2001.

[7] Michael R. Lockwood, "Design and Construction of an Expandable Series Trans-augmented Electromagnetic Railgun," Master's thesis, Naval Postgraduate School, Monterey, California, June 1999.

[8] Jack Bernardes, "Naval Railgun Pulsed Power System Analysis," seminar at the Naval Postgraduate School, Monterey, California, April 2003.

[9] W.F. Weldon and C.W. Drummond, "Compulsators: principles and applications," *Fifth International Conference on Electrical Machines and Drives* (Conf. Publ. No. 341), pp 326-330, September 1991.

[10] J.A. Pappas and D.E. Piccone, "Power Converters for Railguns," *IEEE Transactions on Magnetics*, Vol. 37 Issue: 1, pp. 379-384, January. 2001.

[11] John P. Hartke, "Characterization and Magnetic Augmentation of a Low Voltage Electromagnetic Railgun," Master's thesis, Naval Postgraduate School, Monterey, California, December 1997.

[12] General Atomics Corporation, San Diego, California, Series C capacitors, model number 32327 data sheet, http://www.gaep.com/cspecs.htm, last accessed September 2003.

[13] Ed Goldman, "Vacuum Switch SOA and Improvement Potential," presented at the Electro-Magnetic Launch Workshop, Austin, Texas, November 2001.

[14] Titan Corporation, San Leandro, California, ST-300A Spark Gap switch data sheet, http://www.titanpsd.com/PDFs/St-300.pdf, last accessed September 2003.

[15] Todd Hansen, Silicon Power Corporation, Exton, Pennsylvania, private communication, August 2003.

[16] Silicon Power Corporation, Exton Pennsylvania, SPT-411A data sheet, http://www.siliconpower.com/pdf/spt411a.pdf, last accessed September 2003.

[17] Silicon Power Corporation, Exton Pennsylvania, SDD-303KT datasheet, http://www.siliconpower.com/pdf/sdd303kt.pdf, last accessed September 2003.

[18] Jack Bernardes, Michael F. Stumborg, and Thomas E. Jean, "Analysis of a Capacitor-Based Pulsed-Power System for Driving Long-Range Electromagnetic Guns," *IEEE Transactions on Magnetics*, Vol. 39, No. 1, pp. 486-490, January 2003.

[19] General Atomics Corporation, CCS-12 Charging power supply datasheet.

[20] Akira Yamori, Migiwa Kohno, and Nobuki Kawashima, "Experimental Results of a Two-Stage Plasma Armature Railgun," *IEEE Transactions on Magnetics*, Vol. 39, No. 1, pp. 476-479, January 2003.

INITIAL DISTRIBUTION LIST

1. Defense Technical Information Center
   Ft. Belvoir, Virginia

2. Dudley Knox Library
   Naval Postgraduate School
   Monterey, California

3. Chester Petry
   Naval Surface Warfare Center
   Dahlgren, Virginia

4. Jack Bernardes
   Naval Surface Warfare Center
   Dahlgren, Virginia

5. Dr. Mark Crawford
   Institute for Advances Technology, University of Texas
   Austin, Texas

6. Todd Hansen
   Silicon Power Corporation
   Exton, Pennsylvania

7. CDR Roger McGinnis, USN
   Naval Sea Systems Command
   Washington Navy Yard, DC